THE ASTROPHYSICAL JOURNAL, 536:645–662, 2000 June 20

DIFFUSE IONIZED GAS IN A SAMPLE OF EDGE-ON GALAXIES AND COMPARISONS WITH H I AND RADIO CONTINUUM EMISSION

JOSEPH A. COLLINS, RICHARD J. RAND,[1] AND NEBOJSA DURIC
University of New Mexico, Department of Physics and Astronomy, 800 Yale Boulevard NE, Albuquerque, NM 87131

AND

RENÉ A. M. WALTERBOS
New Mexico State University, Department of Astronomy, MSC4500, Box 30001, Las Cruces, NM 88003
Received 1999 September 29; accepted 2000 January 7

ABSTRACT

We present Hα images of four edge-on galaxies: NGC 5775, NGC 3044, NGC 4183, and NGC 3556. Our goals are twofold: first, to continue the study of the occurrence and physical properties of extraplanar diffuse ionized gas (DIG), and second, to compare extraplanar Hα, H I, and radio continuum emission. The DIG of NGC 5775 is found to be concentrated in numerous bright filaments extending as high as 6 kpc off the midplane. NGC 3044, on the other hand, has a bright, smooth region of DIG above the central part of the disk with some faint filaments at higher galactocentric radius. Vertical profile fits to the extraplanar emission show that both NGC 5775 and NGC 3044 have DIG layers more extended than the Reynolds layer. In contrast, NGC 4183 shows very little extraplanar DIG. Profile fits suggest that it is very unlikely that the DIG layer of NGC 4183 is as extended as the Reynolds layer. The correlation between levels of star formation and prominence of DIG layers for these galaxies is consistent with previous observations. A prediction of the "chimney model" of the ISM is that extraplanar Hα features should have H I and radio continuum counterparts. Comparisons among these three tracers have revealed, for the first time, correlations on the scale of individual extraplanar filaments in a galactic disk. NGC 5775 shows correlations between Hα filaments, H I shells, and radio continuum spurs that are consistent with a chimney model. However, features identified as possible chimneys in NGC 5775 show radio spectral indices steeper than would be expected if cosmic rays were swept into the halo via galactic winds. Calculations of cosmic-ray propagation scale lengths within the DIG filaments demonstrate that diffusion may indeed be responsible for transporting cosmic rays through chimneys marked by DIG filaments. Correlated emission in these three tracers is also seen in NGC 3044, where extraplanar H I and radio continuum features appear to be associated with the galaxy's central region of extraplanar DIG, as well as filaments above the disk. Such correlations are not as prominent in NGC 3556, where extraplanar DIG detection is hampered by the galaxy's relatively low inclination.

Subject headings: diffuse radiation — galaxies: ISM — galaxies: spiral — stars: formation

1. INTRODUCTION

The majority of the ionized component of the interstellar medium (ISM) in the Milky Way is in the form of a vertically extended layer known as the Reynolds layer or warm ionized medium (WIM). The layer has a volume filling fraction of $\gtrsim 20\%$, with a local midplane density of 0.1 cm^{-3}, and a scale height of about 900 pc (Reynolds 1993). Such a medium has also been observed in many external spirals, where it is usually termed diffuse ionized gas (DIG). In face-on spirals, it is a commonly observed feature, appearing as a widespread medium between and around H II regions (e.g., Walterbos & Braun 1994); in edge-ons, widespread emission above the H II region layer is seen only in galaxies with sufficient star formation activity (e.g., Rand 1996). Hence, it would seem that most spirals possess such a medium but the level of star formation probably dictates the thickness of the layer. In many of the edge-ons, the layer is thicker than the Reynolds layer.

The layer is most likely maintained via photoionization by O and B stars since only this source comfortably exceeds the energetic requirements of these ionized layers, both in the Reynolds layer (Reynolds 1993) and external spirals (Walterbos & Braun 1994; Hoopes, Walterbos, & Greenwalt 1996; Ferguson, Wyse, & Gallagher 1996, hereafter FWG96). However, the photoionization picture is not without its problems. First, recent spectroscopic observations of the He I 5876 Å line in the Milky Way (Reynolds & Tufte 1995) and NGC 891 (Rand 1997a) indicate an ionizing spectrum much softer than expected for massive stars. Second, the [O III]/Hβ ratio is found to rise with height off the midplane (z) in NGC 891 (Rand 1998), conflicting with present photoionization models and suggesting a small contribution from a second source such as turbulent mixing layers (Slavin, Shull, & Begelman 1993) or shocks, both of which are ultimately the result of supernova activity. However, it is still unlikely that supernovae are in any way the dominant source of ionization energy for such layers. In the case of the Milky Way, it has been estimated that the maintenance of the Reynolds layer requires nearly all of the supernovae power output (Reynolds 1993).

A third problem, more relevant to this paper, is that for OB associations to be responsible for ionization of such widespread and (often) vertically extended layers, ionizing photons must travel very far from their source. One possible way to produce thick layers of gas in general and to allow ionizing photons to escape the H II region layer is through chimneys. Spatially and temporally correlated supernova and stellar wind activity can drive expanding H I supershells, surrounding relatively evacuated "holes." If suffi-

[1] Visiting Astronomer, National Optical Astronomy Observatories, Tucson, AZ.

ciently energetic, the supershells may break through the gas layers in the disk. The "chimney model" of the ISM, first suggested by Norman & Ikeuchi (1989), predicts that supershells and chimneys may be critical for shaping and energizing the ISM as a whole. Such a structure could provide an unobstructed path for photons to escape the disk and ionize high-z gas. In a galaxy with sufficient star formation distributed over the disk, of order 1000 such chimneys per galaxy are predicted by the model. It is unclear whether such a large number of chimneys exist in a typical spiral. In the nearby spirals M31 (Brinks & Bajaja 1986) and M33 (Deul & den Hartog 1990), about 150 H I holes, which may represent such breakout events, have been cataloged. In edge-ons, at most a few vertical filaments per galaxy have been noted and identified as possible chimneys. Either most chimneys are difficult to recognize or the predicted number is overestimated.

These chimneys also serve as means by which cosmic-ray electrons and magnetic fields can escape into the upper halo, from which synchrotron emission could be detected. Cosmic rays can be transported through chimneys in two ways. The first method is a convective process in which cosmic rays are swept up by thermal gas moving through the chimney. Alternatively, the cosmic rays may simply diffuse through the chimneys and into the halo. The latter process occurs on a larger timescale and leaves a different spectral signature in the radio continuum (Duric, Irwin, & Bloemen 1998, hereafter DIB98). The maintenance of flat spectral index (α) at high z is often taken to be evidence of winds (e.g., Lerche & Schlickeiser 1982). In NGC 5775, DIB98 discovered numerous regions of relatively flat spectral index extending perpendicular to the disk, which were identified as possible chimneys.

Observations of external galaxies support many parts of this theoretical picture. H I holes have been observed in M31 (Brinks & Bajaja 1986) and M33 (Deul & den Hartog 1990), and supershells have been observed in the Milky Way (Heiles 1979, 1984) and many other spirals, including NGC 5775 (Irwin 1994), NGC 4631 (Rand & van der Hulst 1993), NGC 3044 (Lee & Irwin 1997), and NGC 3556 (King & Irwin 1997), although some of the more energetic ones may not be due to multiple supernovae. Extended filaments and shells of Hα emission have been observed in several edge-on spirals (e.g., Rand, Kulkarni, & Hester 1990; Dettmar 1992; FWG96) and interpreted as chimney walls. Radio continuum halos have been detected in numerous external galaxies including NGC 5775 (DIB98), NGC 3044 (Sorathia 1994), and NGC 3556 (Bloemen, Duric, & Irwin 1993, hereafter BDI93). Also, the connection between star formation rates and prominence of DIG layers has been established observationally (Rand, Kulkarni, & Hester 1992, hereafter RKH92; Dettmar 1992; Rand 1996). Multiwavelength comparisons have been performed for only a few galaxies. In NGC 891, asymmetries around the minor axis of the vertical extent of the DIG, H I (Swaters, Sancisi, & van der Hulst 1997), and radio continuum (Dahlem, Dettmar, & Hummel 1994) halos have been found, as well as similarities in the radial extents of the DIG, radio, and X-ray (Bregman & Pildis 1994; Bregman & Houck 1997) halos, suggesting a common production mechanism (Rand 1997b). In addition, comparisons of Hα and X-ray emission in NGC 4631 have revealed similarities in extent along the major axis of the galaxy's DIG and X-ray halos (Wang et al. 1995).

It is clear from the above results that edge-on galaxies are fruitful targets for testing the chimney model. There is little evidence, however, for one important expectation from the chimney model: if chimneys are prevalent and are the main mode of disk-halo gas cycling and vertical cosmic-ray transport, then in edge-ons we might expect to see the signature of individual shells and filaments in multiple ISM tracers. In such a comparison, one is always hampered by the differing resolutions of Hα images versus radio maps and X-ray images, relatively low sensitivity of X-ray observations, and confusion from different regions along a given line of sight. The best such evidence thus far has been reported by Dettmar (1992), who found some correlation between filamentary Hα and 6 cm radio continuum emission features in NGC 5775.

The goal of this paper is twofold: first, to present Hα images of a sample of edge-on galaxies, studying in detail the morphology and occurrence of extraplanar DIG, and second, to compare our Hα data with available high-quality H I and radio continuum maps, attempting to find correlations consistent with a "chimney" model of the ISM. The galaxies for the DIG study have been chosen for their relative proximity and nearly edge-on aspect. Two of the galaxies, NGC 3044 and NGC 4183, were not yet imaged deeply in Hα, while NGC 5775 is included for further study of the above-mentioned correlations. Recent sensitive, high-resolution observations of the 21 cm and radio continuum emission of both NGC 5775 and NGC 3044 allow us to make some of the most detailed comparisons with small-scale Hα structure to date. A spectral index map of NGC 5775 is also included for the comparison. We have also imaged NGC 3556 in Hα on a separate run, as good H I and radio continuum maps are available for our multiwavelength comparison. The observations of these galaxies are discussed in § 2. The Hα images are presented and described in § 3. We model the diffuse emission in § 4, comparing the parameters of the DIG layer to that of the Reynolds layer. The goal of § 5 is to compare our data to available radio maps, attempting to find correlations between the various phases of the ISM. We discuss our results in § 6.

2. OBSERVATIONS

The galaxies were imaged over the course of two runs: at the 0.9 m telescope of Kitt Peak National Observatory in 1997 April and the 3.5 m telescope at Apache Point Observatory[2] (APO) in 1998 March. A summary of the observations is given in Table 1.

For each galaxy, line images were taken through a 28 Å wide filter chosen such that the redshifted Hα line received maximum throughput. The durations of individual line exposures taken at KPNO were typically 30 minutes, while the durations of those taken at APO were 10 minutes. For each line image, an associated continuum image was taken immediately before or afterward for the purpose of continuum subtraction. These were taken through filters of about 75 Å width, covering the continuum adjacent to the Hα and [N II] lines. The resulting KPNO images are flat to $\lesssim$1.5% of sky across regions near the galaxy. The APO images (NGC 3556) are poorly flattened, exhibiting a severe scattered light problem caused by insufficient baffling of the

[2] The APO 3.5 m telescope is owned and operated by the Astrophysical Research Consortium.

TABLE 1

SUMMARY OF OBSERVATIONS

Galaxy	R.A. (J2000.0)	Decl. (J2000.0)	Telescope	Hours of Integration	Hα Filter	EM noise[a] (pc cm^{-6})
NGC 5775.....	14 53 57.6	03 32 40	KPNO 0.9 m	2.8	6600/28	6.6
NGC 3044.....	09 53 40.8	01 34 46	KPNO 0.9 m	4.0	6590/28	4.5
NGC 4183.....	12 13 16.9	43 41 52	KPNO 0.9 m	3.5	6580/28	4.7
NGC 3556.....	11 11 31.8	55 40 15	APO 3.5 m	1.7	6580/28	...

NOTE.—Units of right ascension are hours, minutes, and seconds, and units of declination are degrees, arcminutes, and arcseconds.

[a] Noise levels are for images before any smoothing.

light path in the telescope at the time the data were obtained. Good flattening is unimportant for those observations, however, as their purpose was to find small-scale, filamentary structures. In addition, the field of view of the APO data allowed only the central 13 kpc of NGC 3556's disk to be imaged. Alignment of individual frames was achieved by comparing positions of foreground stars. Flux comparisons of these same stars were used to determine the level of continuum to subtract from the line images. Many of the resulting Hα images show a negative-bowl effect in the bulge region, characteristic of an oversubtracted continuum level. As is often the case, differing stellar populations in the bulge and disk require different levels of continuum subtraction. For our images, we chose a continuum level that we believed appropriate for the disk region. For each galaxy, aligned, continuum-subtracted frames were median averaged to create the final Hα images.

Photometric conditions during the KPNO run allowed a good absolute calibration with the standard stars Feige 34 and BD+33°2642. As a result of time constraints and equipment problems during the APO run, no calibration data were obtained. A rough calibration was obtained for NGC 3556 by using the *R*-band magnitude of the galaxy to calibrate the continuum image, then using fluxes of foreground stars to calibrate the line image. All images were calibrated in ergs cm^{-2} s^{-1} arcsec^{-2} and converted to emission measures (EMs) assuming gas at 10,000 K (an EM of 1 pc cm^{-6} corresponds to 2×10^{-18} ergs cm^{-2} s^{-1} arcsec^{-2} at 10^4 K).

Astrometry was performed on the images with the use of *Hubble Space Telescope* guide stars. The KPNO images typically had many guide stars in the field of view, thus allowing a very accurate determination of a coordinate grid. The small field of view of the APO images contained only two guide stars, the minimum necessary to perform astrometry, albeit with no redundancy. However, the NGC 3556 overlays of Hα and radio data do suggest a fairly accurate astrometric solution.

While the filters typically had a response to the Hα line of ≈90%, they were often broad enough to allow significant [N II] contamination. For the NGC 5775 image, the filter has a ≈75% response to the [N II] line at 6548 Å. In the NGC 4183 frame, the response to the 6548 Å line is ≈90%. Without knowledge of the [N II] λ6583/Hα ratio as a function of height off the midplane, it is very difficult to correct for contamination by [N II]. In NGC 891 for example, the [N II] λ6583/Hα ratio ranges from 0.4 at $z = 0$ to 1.5 at $z = 2.5$ kpc (Rand 1998). Because of these difficulties, we assume the emission measures quoted in § 3 to reflect pure Hα emission. For the modeling in § 4, when the [N II] contribution is judged to be significant, we scale the data by an appropriate factor assuming [N II] λ6583/Hα = 0.5 and [N II] λ6548/[N II] λ6583 = 0.33.

We have VLA radio continuum and H I data for NGC 5775 and NGC 3556. The beam sizes for the NGC 5775 20 cm radio continuum (DIB98) and H I (Irwin 1994) data are 15″ × 13″ and 14″ × 13″, respectively. Beam sizes of the 6 cm radio continuum (BDI93) and H I (J. A. Irwin, private communication) data for NGC 3556 are 32″ × 17″ and 20″ × 12″, respectively. For NGC 3044, Lee & Irwin generously provided VLA 20 cm radio continuum (Sorathia 1994) and H I (Lee & Irwin 1997) data, beam sizes of which are 19″ × 16″ and 21″ × 20″, respectively. We also have a spectral index map of NGC 5775 formed from the 20 and 6 cm radio continuum maps (DIB98).

3. RESULTS

The Hα and continuum images are shown in Figures 1–4. Galaxy parameters, including adopted distances, are given in Table 2. After some brief comments on the general appearance of the galaxies, we will discuss the morphology of extraplanar Hα emission in detail.

3.1. *NGC 5775*

The continuum image of Figure 1 shows a late-type disk with a prominent dust lane on its northeast side. The disk is not quite edge-on, and some spiral structure is evident. An H I bridge connects the northwest edge of the galaxy to its companion, NGC 5774 (Irwin 1994), though no obvious sign of interaction is apparent in the continuum image.

The Hα image of Figure 1 shows much extraplanar DIG, mostly in the form of filaments. The filaments are more prominent in the overlays of Figure 8 where the Hα image has been smoothed to 2″. A smooth, broad layer is apparent in a few locations as well. As mentioned before, the filter has an ≈75% response to the [N II] line at 6548 Å. Thus, with our previous assumptions of line ratios, the contribution from the 6548 Å line is only ≈12% of the total emission. The filaments of NGC 5775 generally have a greater *z*-extent than in previously studied edge-ons. The most prominent plumes, on the eastern side of the disk at $R = 5$–6 kpc north of center, seem to form an incomplete shell-like structure, more apparent in the smoothed image. The filaments extend to nearly $z = 6$ kpc, with an average brightness of about EM = 20 pc cm^{-6}. Two other prominent filaments on the galaxy's west side, one at $R = 9$ kpc north, the other at $R = 5$ kpc south, each average EM = 15 pc cm^{-6} and extend to $z = 4$ and $z = 5$ kpc, respectively.

Also apparent from the Hα image is a possible tidal interaction with NGC 5774. On the southeast side of the galaxy,

TABLE 2

GALAXY PARAMETERS

Galaxy	Type	Distance (Mpc)	Adopted Inclination (deg)	L_{FIR} ($\times 10^{43}$ ergs s^{-1})	L_{FIR}/D_{25}^2 ($\times 10^{40}$ ergs s^{-1} kpc^{-2})
NGC 5775.....	Sc	24.8	86	7.9	8.4
NGC 3044.....	Sc	16.14	85	1.8	3.5
NGC 3556.....	Scd	11.6	78	2.5	3.2
NGC 4183.....	Sc	17.0	84	...[a]	...

NOTE.—Values of D_{25} are from de Vaucouleurs et al. 1991.

[a] NGC 4183 is not included in the *IRAS* survey.

REFERENCES FOR DISTANCES AND INCLINATIONS.—NGC 5775: Irwin 1994; NGC 3044: Lee & Irwin 1997; NGC 3556: King & Irwin 1997; NGC 4183: Tully 1988 and IPAC.

a number of compact sources, presumably H II regions, are located at heights up to $z = 5$ kpc off the midplane, indicating that star formation may be occurring well above the disk. In addition, on the galaxy's northwest side, an isolated H II region is at a height of $z = 5$ kpc. Another isolated H II region is located 10 kpc northwest of the galaxy's northwest edge. Irwin (1994) has suggested that star formation may be occurring between the two galaxies. The detection of these isolated H II regions seems to suggest this is a likely scenario.

3.2. *NGC 3044*

The continuum image shown in Figure 2*a* shows a nearly edge-on disk with a prominent dust lane appearing on the southern edge of the galaxy. The image shows a possible asymmetric distribution of matter, as the northwest side of the galaxy appears significantly brighter than the southeast side.

This asymmetry is even more apparent in the Hα image of Figure 2*a*, as the southeastern side shows very little emis-

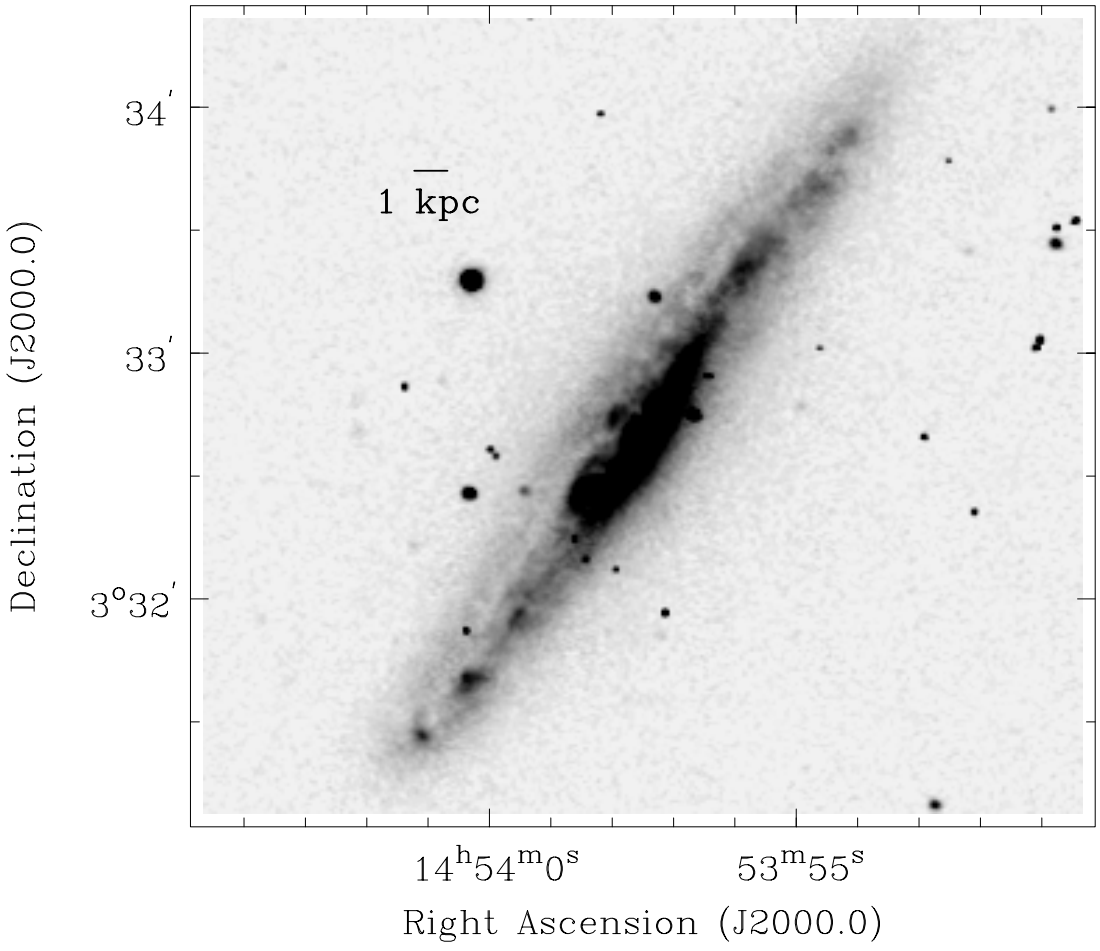

FIG. 1*a*

FIG. 1.—Images of NGC 5775 in (*a*) red continuum and (*b*) continuum-subtracted Hα

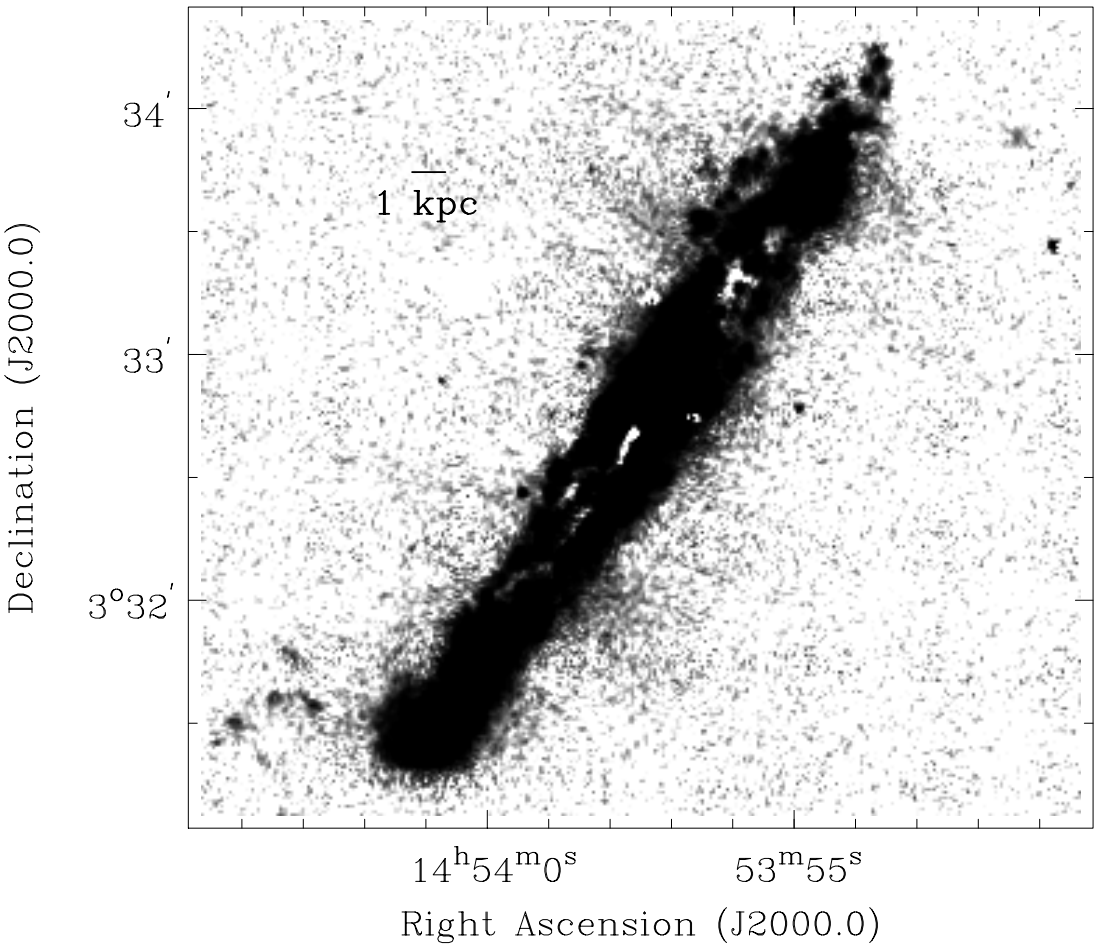

FIG. 1*b*

sion, caused in part by an oversubtracted continuum level. However, even if the continuum subtraction were correct in this region, the asymmetry would still exist. The asymmetry is not due to poor response of the filter to emission on the southeast, receding side of the galaxy. Emission on both the northwest (approaching) and southeast sides of the galaxy are within the filter's peak response region. The image has very little [N II] contamination, as the throughput of both lines is low. The diffuse emission can be better seen in the overlays of Figure 10 where the image has been smoothed to 2″. The image shows extensive diffuse emission concentrated mainly above the bulge of the galaxy, possibly tracing out a central starburst. This region covers about 7 kpc of the disk around the bulge and is detectable out to $z = 4$ kpc above and below the disk. At $z = 1$ kpc, the brightness of the layer averages about EM = 25 pc cm^{-6}. At $R = 1$–2 kpc on the northwestern side, a prominent shell extends to a height of about $z = 1.5$ kpc below the disk. The filaments in the shell average around EM = 35 pc cm^{-6} and appear to form a nearly closed loop, as seen in Figure 2*b*. However, the shell is fairly clumped in appearance and may just be a collection of H II regions below the midplane. Faint emission is present outside of the central region as well, with the most extended filament, at $R = 5$ kpc on the northwestern side, extending to about $z = 4$ kpc above the disk.

3.3. *NGC 4183*

The continuum image of Figure 3 shows a prominent bulge with a faint, nearly edge-on disk. A faint dust lane is visible on the western edge of the galaxy.

The throughput of the [N II] line at 6548 Å is $\approx$90% for the Hα image. Thus, under our assumptions, [N II] emission is responsible for $\approx$15% of the brightness in the image. The image shows a collection of H II regions in the disk but no evidence for an extraplanar diffuse layer. The brightness at $z = 1$ kpc is only a few pc cm^{-6}. The only extraplanar feature is a faint plume at $R = 7$ kpc north, which extends to $z = 2$ kpc east, with an average brightness around EM = 10 pc cm^{-6}.

3.4. *NGC 3556*

The continuum image of Figure 4 shows a late-type disk with a fairly prominent bulge. Prominent dust features are visible along the northern side of the galaxy. Spiral structure is clearly visible in the disk, demonstrating that this galaxy is not as edge-on ($i = 78°$ as measured by King & Irwin 1997) as the others in our sample.

The Hα image has very little [N II] contamination, as the throughput of the [N II] lines is low. The relatively low inclination of the galaxy coupled with the poor flattening make it difficult to detect a widespread extraplanar layer. A

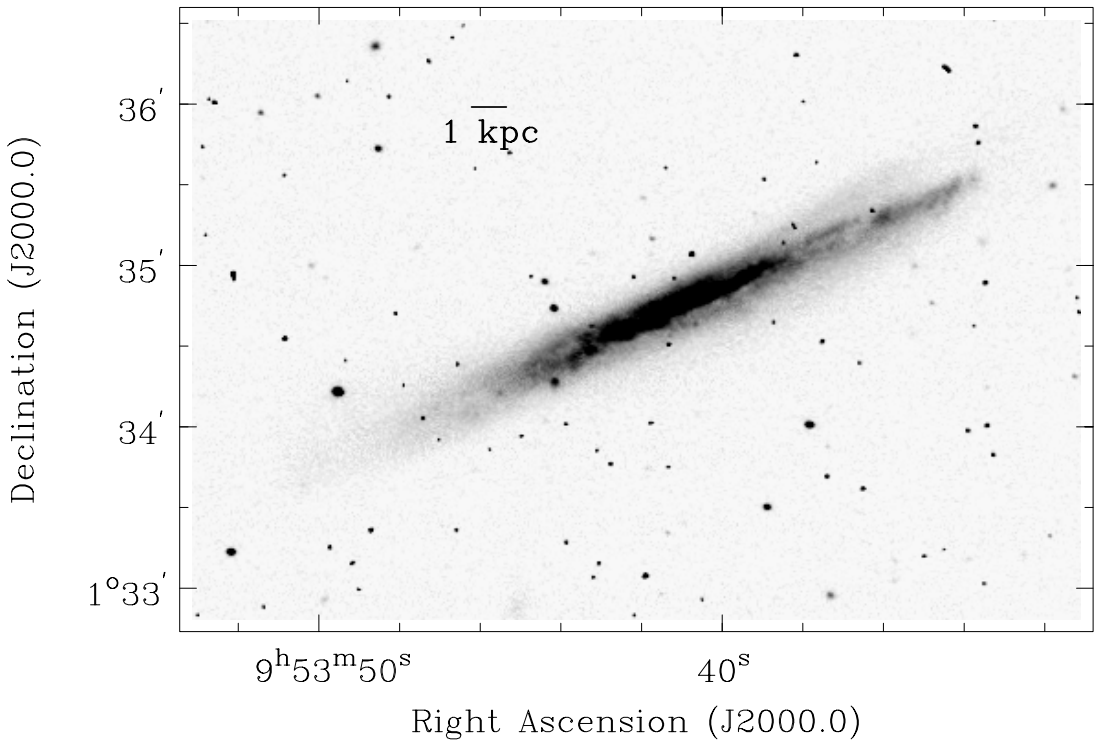

FIG. 2*a*

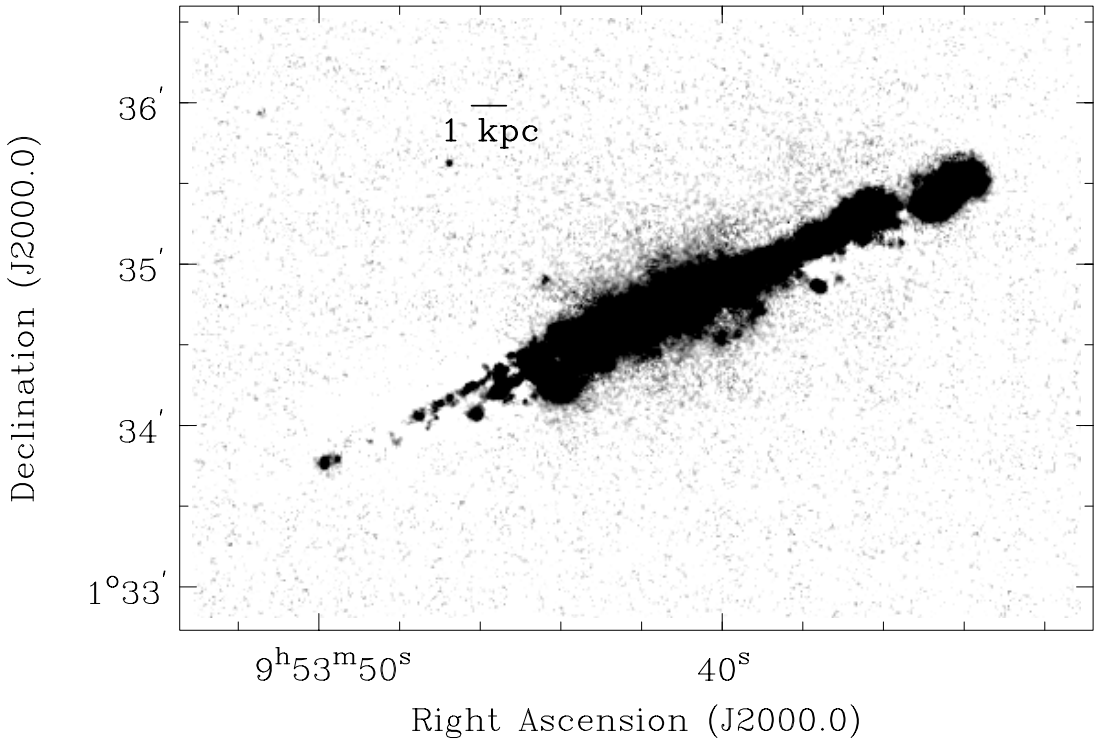

FIG. 2*b*

FIG. 2.—Images of NGC 3044 in (*a*) red continuum and (*b*) continuum-subtracted Hα. (*c*) Close-up of the loop on the southern side of NGC 3044. The image has been smoothed to 1.″5.

DIG layer extending to $z = 1$ kpc in a galaxy inclined greater than 10° would be almost entirely projected onto the disk. There is, however, much diffuse emission between H II regions in the disk. This emission is likely due to a combination of extraplanar and in-plane DIG. Some of the emission on the eastern side of the galaxy does appear to be extraplanar. One interesting feature, a prominent loop of extraplanar gas at $R = 3$ kpc east of center, extends about

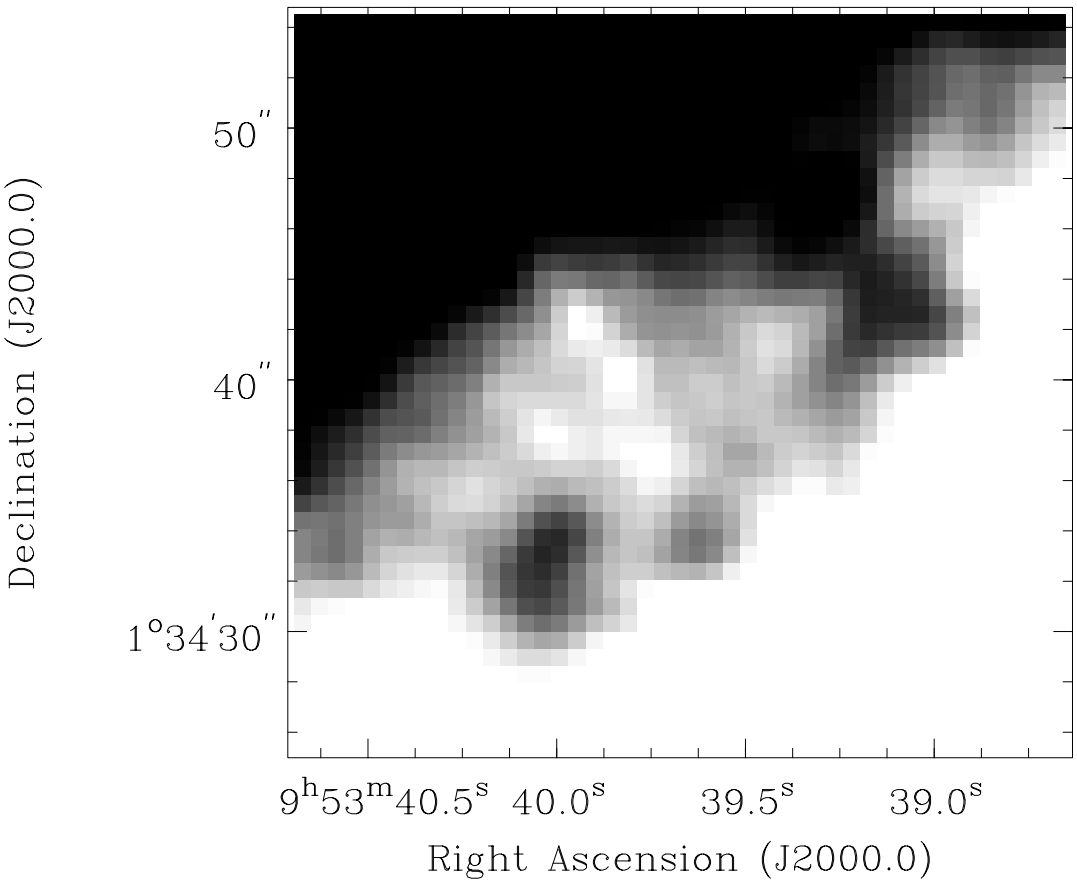

FIG. 2*c*

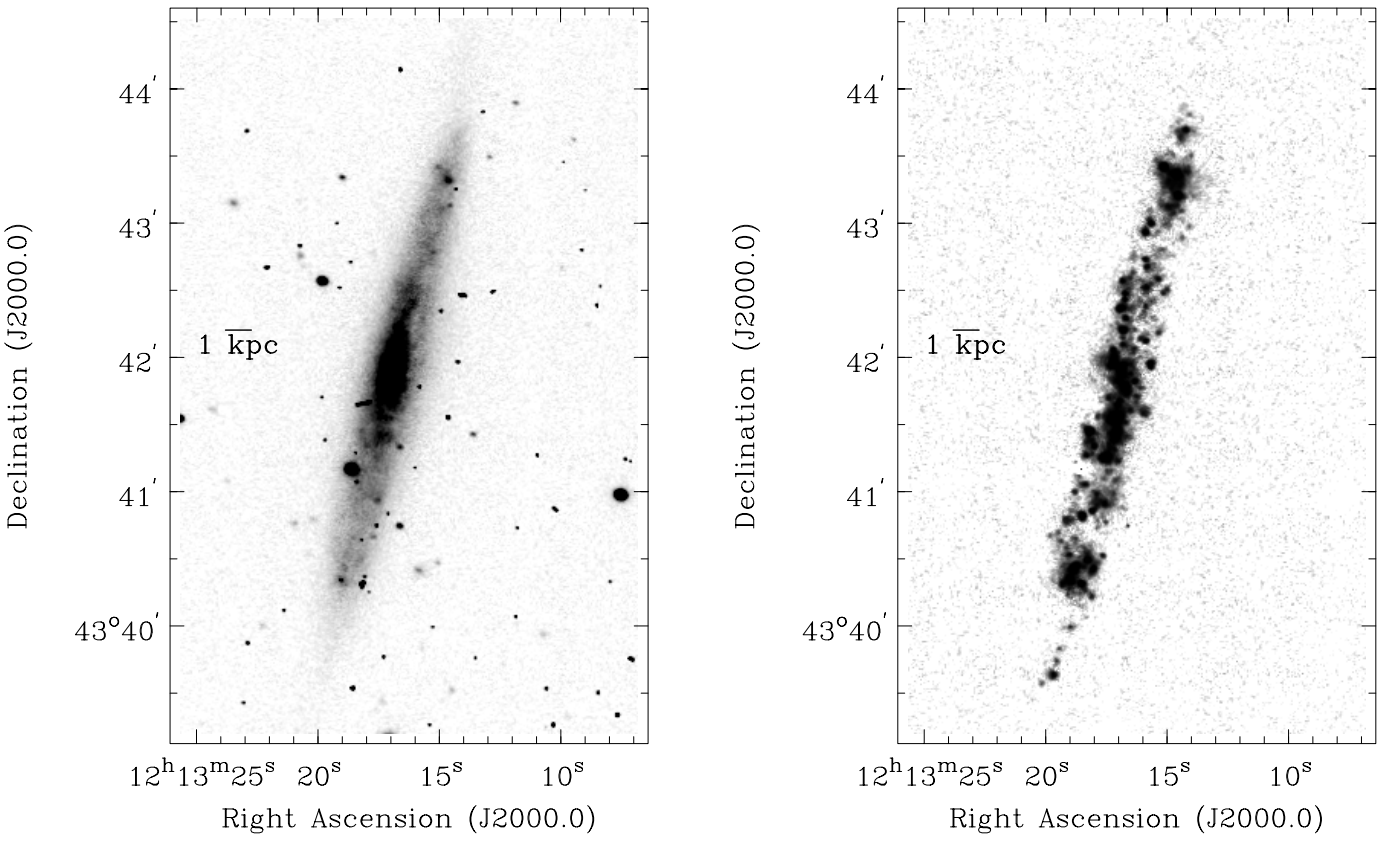

FIG. 3.—Images of NGC 4183 in (*left*) red continuum and (*right*) continuum-subtracted Hα

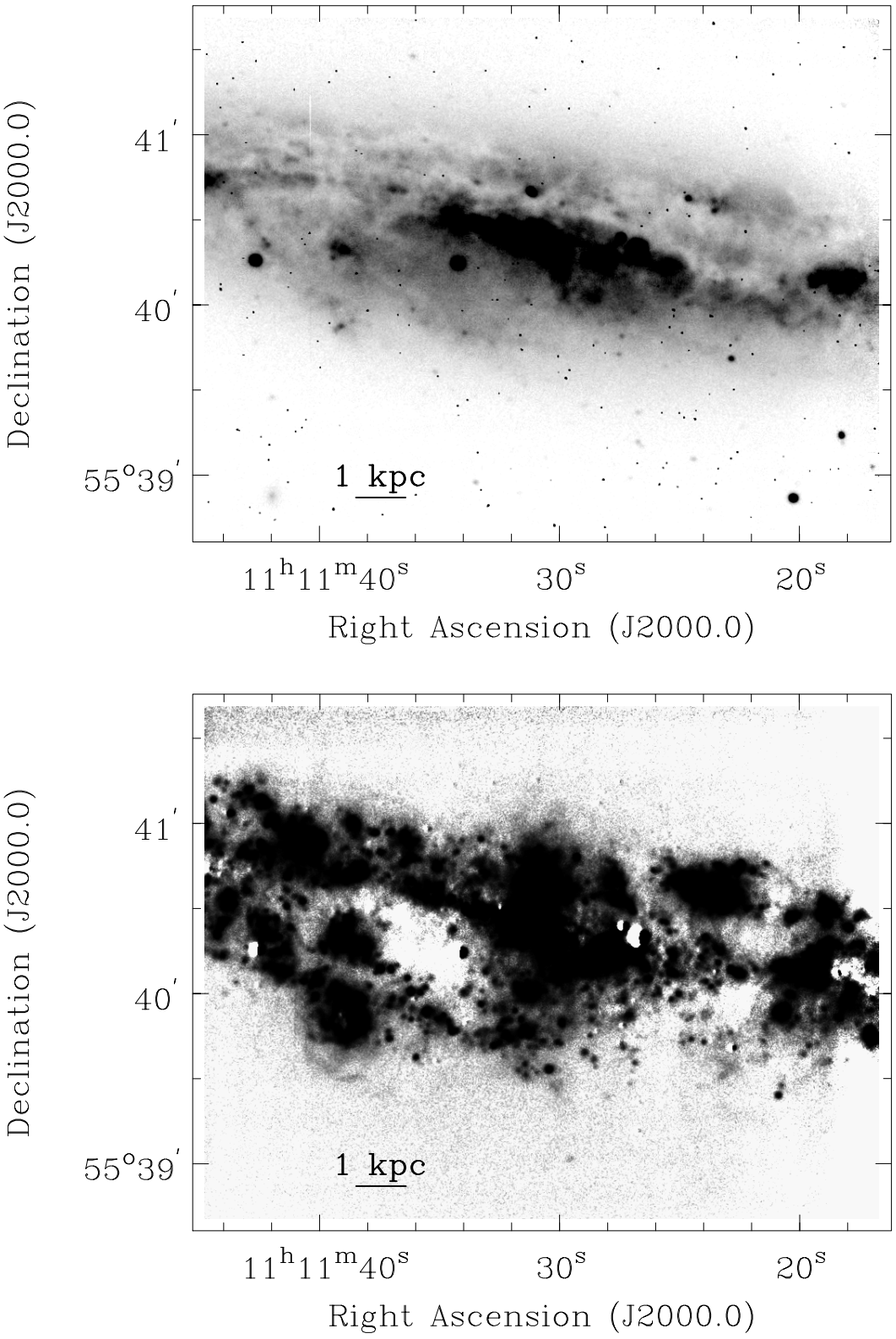

FIG. 4.—Images of NGC 3556 in (*top*) red continuum and (*bottom*) continuum-subtracted Hα

26″ to the south of a cluster of H II regions in the disk. If we assume this angular distance is entirely in the z-direction, the loop extends to a height of about $z = 1.5$ kpc. On the northeast side of the galaxy, there is much diffuse emission that appears to extend above H II regions in the disk, parallel to the minor axis. The most prominent filaments extend from the central region to a height of about $z = 1.5$ kpc, assuming the angular extent is entirely in the z-direction.

4. MODELING THE DIFFUSE EMISSION

Of the calibrated data we have obtained, NGC 5775 and NGC 3044 show clear signs of extraplanar DIG. In this

section, for each galaxy (except NGC 3556), we attempt to determine the parameters of an extended, smooth layer of ionized gas that are consistent with the data. In addition, for NGC 4183, which shows no clear sign of a smooth component in our data, we attempt to determine whether the galaxy could be hiding a layer with the properties of the Reynolds layer. Parameters such as the midplane density, scale height, radial distribution, temperature, and filling factor of the gas, as well as the inclination of the galaxy, all affect the appearance of such a layer. Following Rand (1996) and Hoopes, Walterbos, & Rand (1999), our method considers a simple model with a midplane density constant with R and a single exponential in the z-direction for each vertical profile. The model extends to an outer radius, R_0, the value of which is chosen depending on the goals of the modeling. The model is placed at the inclination quoted in Table 2, and a model profile, averaged over a specific range along the major axis, is generated. We take the local Reynolds layer distribution as the standard for comparison. This we call the "standard model," for which the scale height (H) of the emission is taken to be 450 pc and $\langle n_e^2 \rangle_0$, the mean of n_e^2 on the midplane, is taken as 0.007 cm^{-6}.

Since our goal is to model an extended diffuse layer, we take vertical profiles from the NGC 5775 and NGC 3044 images where the extraplanar layer is fairly smooth in appearance, with little or no filamentary structure. The profiles typically cover a 1–2 kpc radial extent of the disk and are averaged over that range. If [N II] contamination is judged to be significant, we scale the data by an appropriate factor assuming line ratios given in § 2. If the [N II] λ6583/Hα ratio in fact rises with height off the midplane, then DIG scale heights will be slightly overestimated depending on the level of [N II] throughput. We fit by eye, attempting to fit the model to the data above the H II region layer and any dust lane present (to avoid the problem of extinction).

Byun, Freeman, & Kylafis (1994) have modeled optical extinction in spiral galaxies, assuming a ratio of dust to stellar scale height of $z_d/z_s = 0.4$. For the highest central, face-on, V-band optical depth considered ($\tau_v = 10$), the model's prediction for a galaxy inclined 85° is peak extinction at $z \approx z_s/3$, with extinction effects becoming negligible at $z \approx 2z_s/3$ on the near side of the galaxy, with little attenuation on the far side. In NGC 5775, which is inclined to 86°, peak extinction occurs at $z \approx 300$ pc (see Fig. 5). Thus, extinction effects should become negligible at $z \approx 600$ pc. Since our model profiles typically do not converge with the measured profiles until well above $z = 1$ kpc, extinction effects on the profiles should be negligible. The ratio z_d/z_s may be higher, though it is not clear whether such a scenario is appropriate. The effect of an increased ratio, however, would be offset by a more realistic choice of τ_v.

We also avoid fitting the H II region layer in the disk because of the uncertain correction necessary for extinction. By neglecting contributions from the H II region layer, one could argue that the faint wings of the central distribution contaminate the DIG model. This problem is minimized by fitting the DIG layer at relatively high z. In any case, the presence of faint wings of a central exponential emission distribution would result in an underestimated DIG scale height.

The midplane of the galaxy, determined from the images, is taken as the center of the model. In a few cases, the models do not appear centered on the observed profiles. This can happen when bright H II regions located just off the major axis make significant contributions to the emission profile.

Given that extraplanar DIG generally does not extend smoothly along the entire length of the major axis as implicitly assumed in the models, particularly for NGC 5775, the radial distribution is poorly constrained, and thus so are derived values of $\langle n_e^2 \rangle_0$. Our primary interest is in modeling the vertical extent.

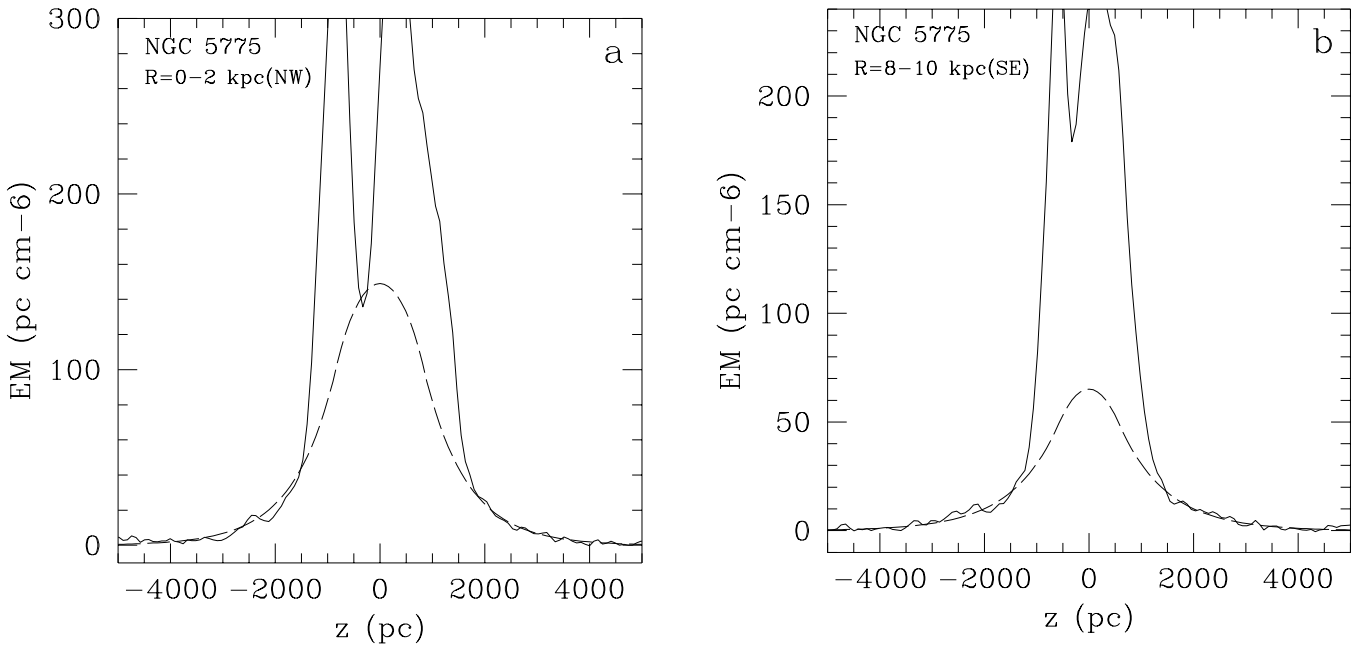

FIG. 5.—Vertical profiles for NGC 5775. Positive z corresponds to the southwest side. (*a*) Vertical profile for $R = 0$–2 kpc on the northwest side (*solid line*) and a model with $\langle n_e^2 \rangle_0 = 0.010$ cm^{-6}, $H = 800$ pc, and $R_0 = 12$ kpc (*dashed line*). (*b*) Vertical profile for $R = 8$–10 kpc on the southeast side (*solid line*) and a model with $\langle n_e^2 \rangle_0 = 0.0055$ cm^{-6}, $H = 900$ pc, and $R_0 = 12$ kpc (*dashed line*).

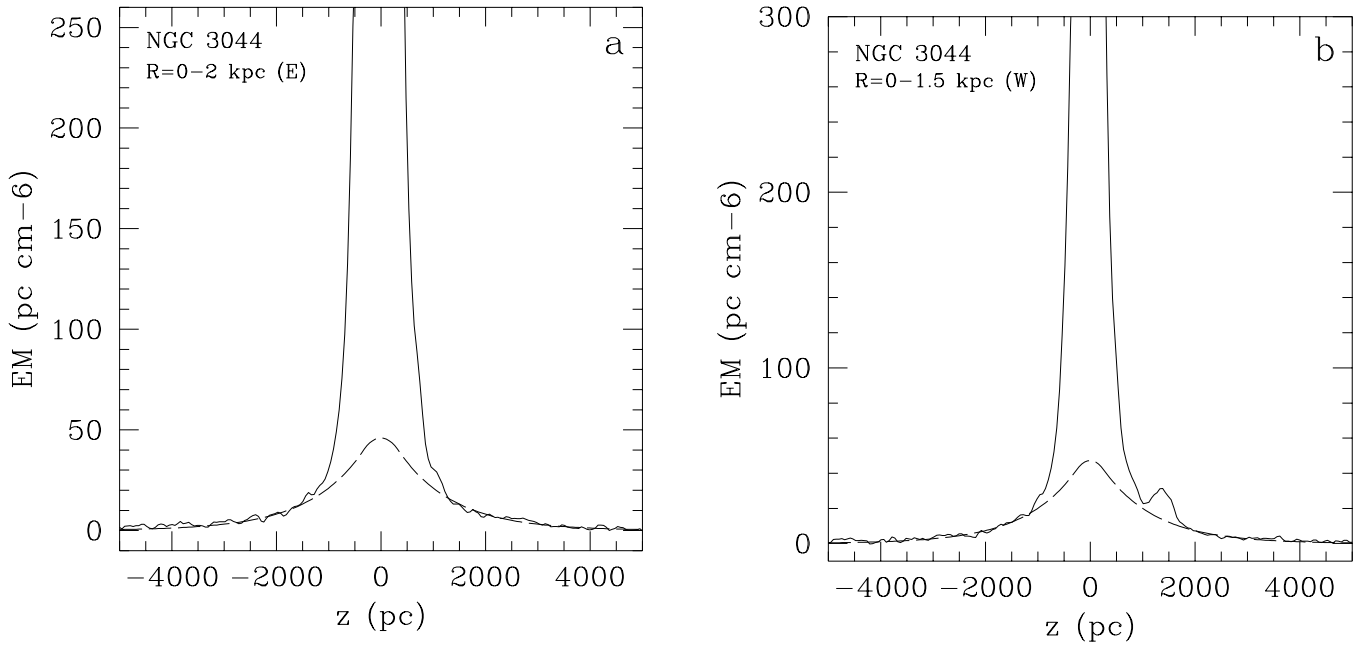

FIG. 6.—NGC 3044 vertical profiles. Positive z corresponds to the south side. (*a*) Vertical profile for $R = 0$–2 kpc on the east side (*solid line*) and a model with $\langle n_e^2 \rangle_0 = 0.007$ cm^{-6}, $H = 1050$ pc, and $R_0 = 4$ kpc (*dashed line*). (*b*) Vertical profile for $R = 0$–1.5 kpc on the west side (*solid line*) and a model with $\langle n_e^2 \rangle_0 = 0.009$ cm^{-6}, $H = 1000$ pc, and $R_0 = 4$ kpc (*dashed line*).

4.1. *NGC 5775*

As mentioned previously, the [N II] 6548 Å line has a throughput of $\approx 75\%$. The stronger [N II] 6583 Å line has less than 5% throughput and thus makes a negligible contribution to the total brightness. Thus, we scale the vertical profiles assuming [N II] contributes 12% to the total brightness. We use the value from Irwin (1994) of $i = 86°$. The galaxy has much extraplanar emission, but mainly in the form of filaments. Nevertheless, there are some extended regions of relatively smooth emission between the filaments. Because of the widespread nature of the extraplanar DIG, we assume $R_0 = 12$ kpc, the size of the Hα-emitting disk.

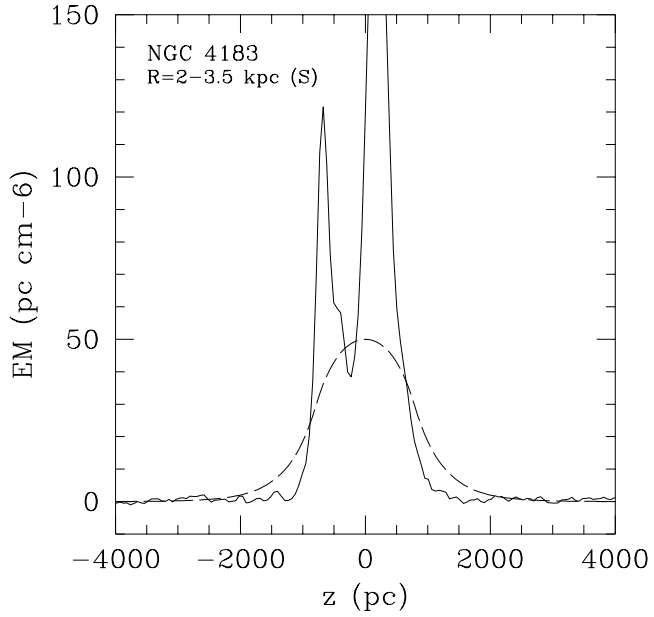

FIG. 7.—Vertical profile for $R = 2$–3.5 kpc on the south side of NGC 4183 (*solid line*) and the standard model with $R_0 = 8$ kpc (*dashed line*). Positive z corresponds to the west side.

Near the center of the disk, at $R = 0$–2 kpc to the northwest, a smooth region of extraplanar gas occurs on the southwest side. The profile for this region is shown in Figure 5*a*. We do not model the northeast side ($-z$), as the emission in that area has a mainly filamentary morphology. The profile for the southwest side ($+z$) is well fitted by a range of parameters, from $\langle n_e^2 \rangle_0 = 0.010$ cm^{-6} and $H = 800$ pc (the model shown) to $\langle n_e^2 \rangle_0 = 0.0065$ cm^{-6} and $H = 900$ pc.

Another region of relatively smooth emission occurs at $R = 8$–10 kpc on the southeast side. The profile for this region, along with a model that fits the profile well, are shown in Figure 5*b*. The model shown has $\langle n_e^2 \rangle_0 = 0.0055$ cm^{-6} and $H = 900$ pc. Models that deviate much from these values produce poor fits.

4.2. *NGC 3044*

The throughput of the [N II] lines is low: that of the [N II] 6548 Å line is $\lesssim 40\%$, while the stronger [N II] 6583 Å line is $\approx 10\%$. Thus, we ignore [N II] emission in modeling the profiles. The Lee & Irwin (1997) value of $i = 85°$ is used for the model. We concentrate on modeling the central region where a bright, smooth extraplanar layer of DIG occurs.

A profile within this central region, at $R = 0$–2 kpc on the east side, is shown in Figure 6*a*. For the model, we take $R_0 = 4$ kpc, the radial half-width of the extended layer. A range of parameters provide a good fit to the profile, from $\langle n_e^2 \rangle_0 = 0.007$ cm^{-6} and $H = 1050$ pc (the model shown) to $\langle n_e^2 \rangle_0 = 0.004$ cm^{-6} and $H = 1500$ pc.

The profile for $R = 0$–1.5 kpc on the west side is shown in Figure 6*b*. This profile is also within the central region of extended emission; thus, we again assume $R_0 = 4$ kpc. A prominent shell extends off the disk to the south ($+z$) side, seen as a prominent spike in the profile at $z = 1500$ pc. Thus, we model only the north ($-z$) side, where parameters ranging from $\langle n_e^2 \rangle_0 = 0.006$ cm^{-6} and $H = 1200$ pc to

$\langle n_e^2 \rangle_0 = 0.009$ cm^{-6} and $H = 1000$ pc (the model shown) fit the profile well.

4.3. *NGC 4183*

The [N II] 6548 Å line has ≈90% throughput, while the throughput of the [N II] 6583 Å line is near 0. Thus, we scale the profile assuming a 15% contribution to the total brightness from [N II] emission. The disk is not quite edge-on, so we use the value listed in the UGC catalog, $i = 84°$. For the modeling, we concentrate on determining whether the galaxy could be hiding a smooth, extended layer with parameters comparable to the Reynolds layer.

The profile shown in Figure 7, at $R = 2$–3.5 kpc on the south side, is for a typical region of the disk. The dip in the central part of the profile is due more to a gap in the H II region layer than an oversubtracted bulge. For the model, we choose a layer of $R_0 = 8$ kpc, the radial extent of the Hα-emitting disk. We also assume the parameters of our "standard model," $\langle n_e^2 \rangle_0 = 0.007$ cm^{-6} and $H = 450$ pc. The model clearly overestimates the amount of extraplanar emission. In fact, the profile shows little emission outside of the H II region layer whatsoever. Thus, it is fairly unlikely that the galaxy contains a smooth, extended layer with parameters comparable to the Reynolds layer.

5. COMPARISON OF Hα, H I, AND RADIO CONTINUUM DATA

5.1. *Multiwavelength Comparison of Extraplanar Features*

The galaxies NGC 5775, NGC 3044, and NGC 3556 all exhibit features of extraplanar DIG. In this section, we compare our Hα data with available radio continuum and H I data, with a goal of correlating features of the various phases of the ISM. Because of the two-dimensional nature of our data, however, extraplanar features cannot be conclusively correlated. In addition, because of extinction in the disk, it is very difficult to correlate extraplanar features with optical activity in the H II region layer. The disk is transparent to radio wavelengths, however, for which radio hot spots may mark the location of star-forming regions. Our approach is purely qualitative. We look for general correlations of halo structure as well as specific features that might mark the locations of chimneys.

5.1.1. *NGC 5775*

Radio continuum observations performed by DIB98 have detected an extensive halo that is detectable to a diameter along the minor axis of 10–15 kpc. Model fits to the continuum emission reveal a disk component of scale height 1 kpc and a halo component of scale height 3.5 kpc. Irwin (1994) has performed an extensive observation of the galaxy's H I emission and reports that H I and radio continuum features, though not well correlated spatially, do appear to be "associated" with one another. Correlations between Hα and radio continuum filaments have been reported by Dettmar (1992), though his radio data were of lower sensitivity and poorer resolution than our data. The H I column density and 20 cm radio continuum contour maps are shown in Figure 8, overlain on the Hα image. Arrows indicate locations of possible chimneys. The beam sizes of the H I and radio continuum maps are 14″ × 13″ and 15″ × 13″, respectively. The Hα image has been smoothed with a 2″ Gaussian to enhance the filamentary emission.

In all three tracers, the halo appears very bright and extended. In addition, the radio maps of NGC 5775 show many extraplanar shells and filaments, as well as a bright disk. A bright radio hot spot in the disk, at $R = 5$ kpc on the south side, seems to mark a region of intense star formation as prominent DIG filaments extend to either side of the disk at this location. Radio hot spots in the disk are also found below the DIG filament on the west side of the disk at

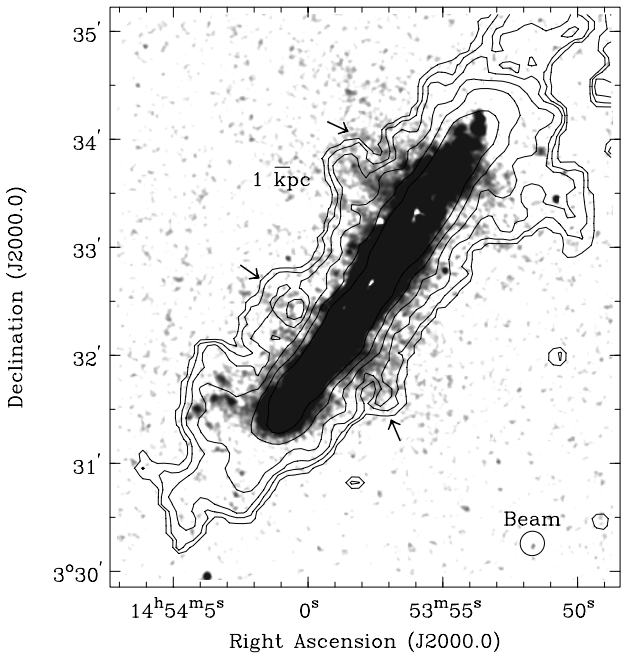

FIG. 8*a*

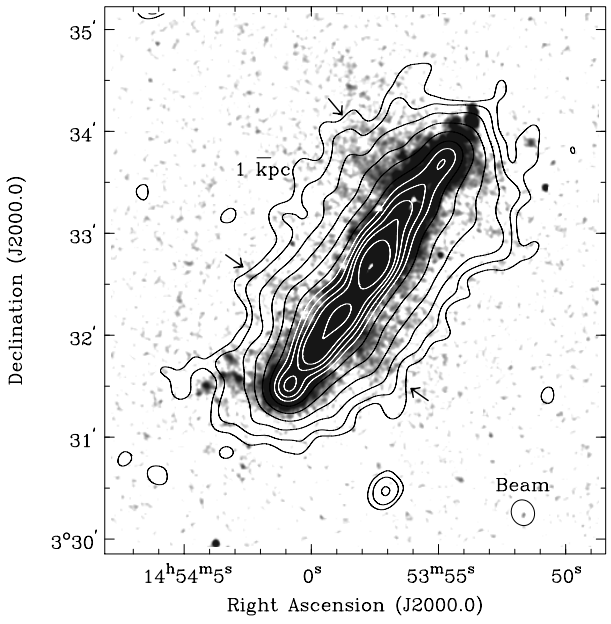

FIG. 8*b*

FIG. 8.—Hα image of NGC 5775, smoothed to 2″ resolution, with contour overlays of (*a*) H I emission and (*b*) 20 cm radio continuum emission. Arrows indicate locations of possible chimneys. Contours for the H I map are 1, 4, 8, 16, 30, and 50 times 10^{20} cm^{-2}. Contours for the radio continuum map are 1, 2, 4, 8, 16, 32, 48.4, 64, 82.2, 100, and 137 times 95 μJy beam^{-1}.

$R = 9$ kpc north of center, as well as below the collection of H II regions and diffuse gas at the far southern end of the galaxy.

More so than the other two galaxies discussed in §§ 5.1.2 and 5.1.3, the correlations between the various phases of the extraplanar ISM seem to be consistent with a "chimney model." The most prominent Hα filaments, extending to the east at $R = 5$–6 kpc on the north side, appear to be well correlated with a neutral hydrogen feature. The fact that the Hα filaments seem to form a shell within a pair of prominent H I extensions is strongly suggestive of a chimney structure. A radio continuum spur is located in this part of the halo as well. The bright filament extending to the west at $R = 5$ kpc on the south side appears to be associated with a prominent H I structure, identified by Irwin (1994) as an H I shell, though the features are slightly offset from one another. Again, this region of emission is associated with a radio continuum spur. A large H I feature east of the disk at $R = 5$ kpc south of center, identified by Irwin (1994) as an H I shell, seems to be correlated with a faint, yet extended Hα filament. The filament is well aligned with another radio continuum spur. A large plume of DIG on the west side at $R = 9$ kpc north of center is associated with an extended H I spur as well as small radio continuum filaments. However, the extraplanar emission at this location could be the result of a gravitational interaction with the companion galaxy, as suggested by Irwin (1994), instead of a disk-halo interaction. Finally, on the east side of the disk's far southern edge, a collection of H II regions and diffuse gas extends far off the disk. Also in this region, the radio maps show an extended plume of H I gas and a radio continuum spur, which could have arisen through a tidal interaction as well.

The spectral index map of NGC 5775 is shown in Figure 9*a*. Figure 9*b* shows the smoothed Hα image of NGC 5775 with spectral index contours. Because of the complexity of the spectral index map, we show only two contours: emission within the white contour has the flattest spectral index ($\alpha < 0.8$), while emission within the black contours has the steepest ($\alpha > 1.1$). Contrary to previous suggestions that convection is the main mode of CR transport through chimneys, our data suggests that this is not the case in chimneys marked by DIG filaments. Each of the features we have identified as a possible chimney, marked with arrows in Figure 9*b*, is characterized by a relatively steep spectrum. A steep spectral index in the halo is expected if cosmic rays, instead of being swept out of the disk with thermal gas, are allowed to diffuse into the halo. The possibility of cosmic rays diffusing through chimneys into the halo is explored in § 6.2.1.

5.1.2. *NGC 3044*

NGC 3044 has been observed in H I by Lee & Irwin (1997), who detected numerous neutral hydrogen spurs and supershells. Radio continuum emission has been detected up to $z = 8$ kpc by Sorathia (1994). Lee & Irwin report that H I and radio continuum emission, in many cases, do appear to be well correlated. Figure 10 shows the Hα image, with H I column density and 20 cm radio continuum contour overlays. Beam sizes of the H I and radio continuum maps are $21'' \times 20''$ and $19'' \times 16''$, respectively. To enhance filamentary emission, the Hα image has been smoothed with a $2''$ Gaussian.

It is interesting that the Hα and radio continuum halos have a very similar structure in general. In fact, the Hα-emitting disk and radio continuum halo terminate at the same radial location, though the H I disk continues to the east. This is consistent with a model where cosmic rays in the upper halo have their source in the supernova-rich H II region layer. In addition, a radio-bright region of the disk, at $R = 5$ kpc west of center, likely marks a star-forming region, as both an extraplanar DIG filament and an H I supershell originate at this location.

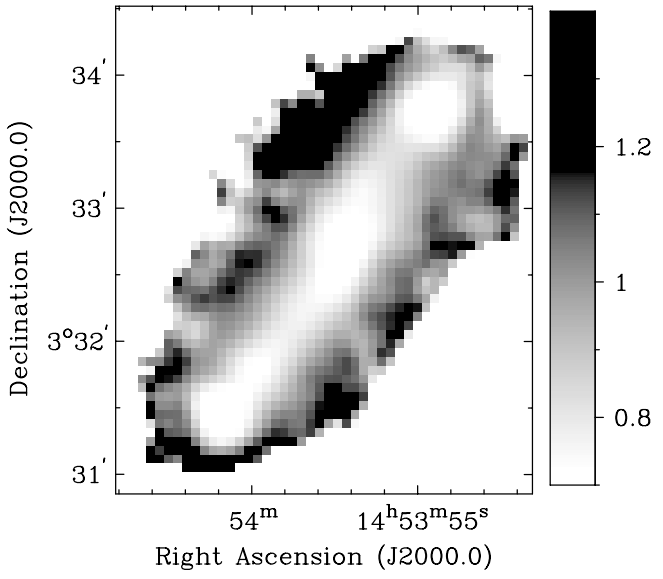

FIG. 9*a*

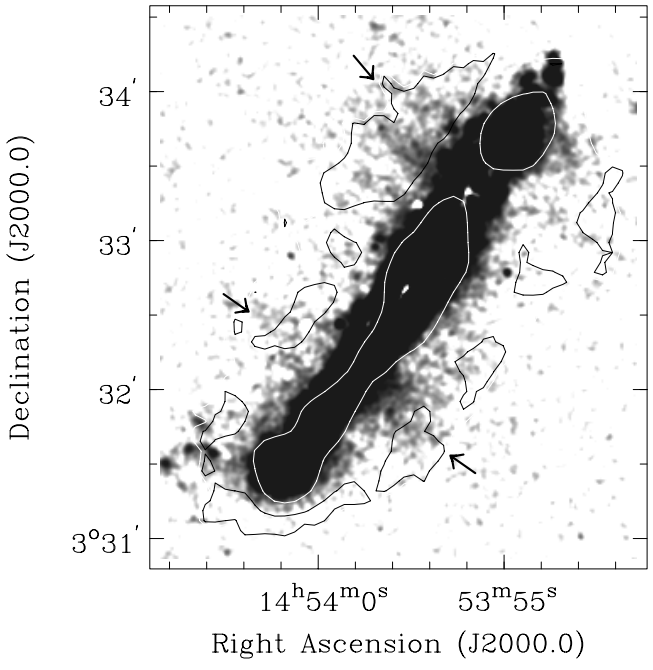

FIG. 9*b*

FIG. 9.—(*a*) Spectral index map of NGC 5775. Gray-scale values are shown in the color bar. (*b*) Hα image of NGC 5775, smoothed to $2''$ resolution, with spectral index contours. The white contour corresponds to $\alpha = 0.8$, while the black corresponds to $\alpha = 1.1$. Arrows mark the locations of possible chimneys.

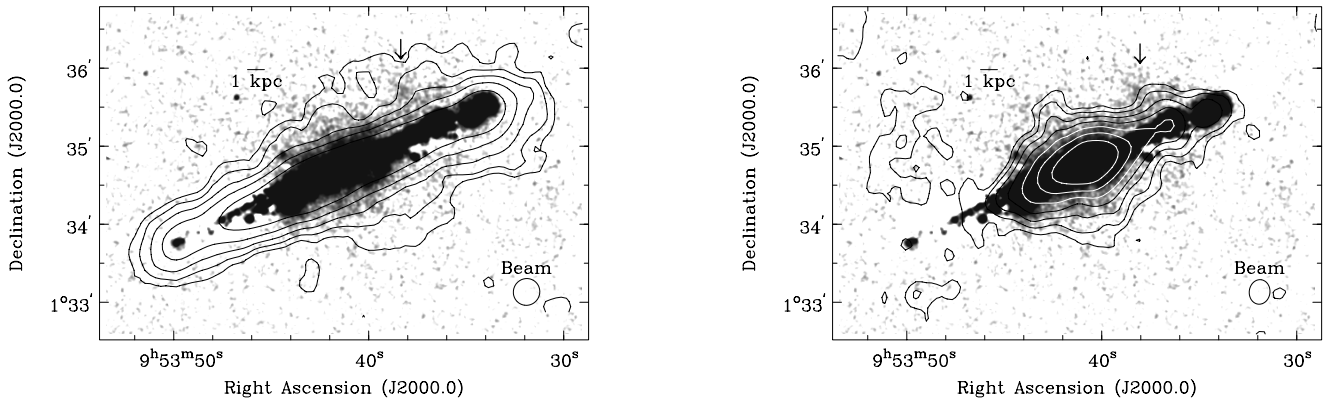

FIG. 10.—Hα image of NGC 3044, smoothed to 2″ resolution, with contour overlays of (*top*) H I emission and (*bottom*) 20 cm radio continuum emission. The arrow marks the location of a possible chimney. Contours for the H I map are 1, 2, 4, 8, and 16 times 76 Jy Hz beam^{-1}. Contours for the radio continuum map are 1.1, 2.2, 4.4, 8.8, 17.8, 35.2, and 70.4 times 100 μJy beam^{-1}.

The bright central region of extraplanar DIG can be correlated with H I and radio continuum features. The southern spur of enhanced H I column density appears associated with the central region of DIG, though they are slightly offset. Within this area, the loop of Hα emission, better seen in Figure 2*b*, is in the proximity of a feature identified as an expanding H I supershell. The Hα loop is centered at a position 23″ north and 4″ east (or 1.8 kpc) of the center of the H I supershell. There appears to be some overlap of these features, as the radius of the Hα loop is roughly 1 kpc, while the H I shell has a radius of 1.7 kpc (Lee & Irwin 1997). A spur of enhanced radio continuum emission passes through this region as well. North of the disk, two H I spurs occur above the central region of DIG, where a prominent radio continuum spur also originates. The northern H I feature at $R = 5$ kpc west of center, identified by Lee & Irwin as the most massive and energetic of the H I supershells, is associated with a faint filament of DIG as well as a radio continuum spur. In displaying correlations between the three tracers, this feature, marked with an arrow in Figure 10, is the most likely candidate for a chimney in this galaxy.

5.1.3. *NGC 3556*

King & Irwin (1997) have performed an H I survey of NGC 3556, discovering a number of neutral hydrogen shells and extensions. Observations by BDI93 have detected a radio continuum halo. The Hα image, both the unsmoothed version and one smoothed to 1.5″ resolution, are shown in Figure 11, with contour overlays of H I column density and 6 cm radio continuum. The beam size of the H I map is 20″ × 12″, while the radio continuum map has a 32″ × 17″ beam size.

As mentioned previously, the low inclination of NGC 3556 makes the identification of any but the most extended DIG features for comparison to radio features very difficult.

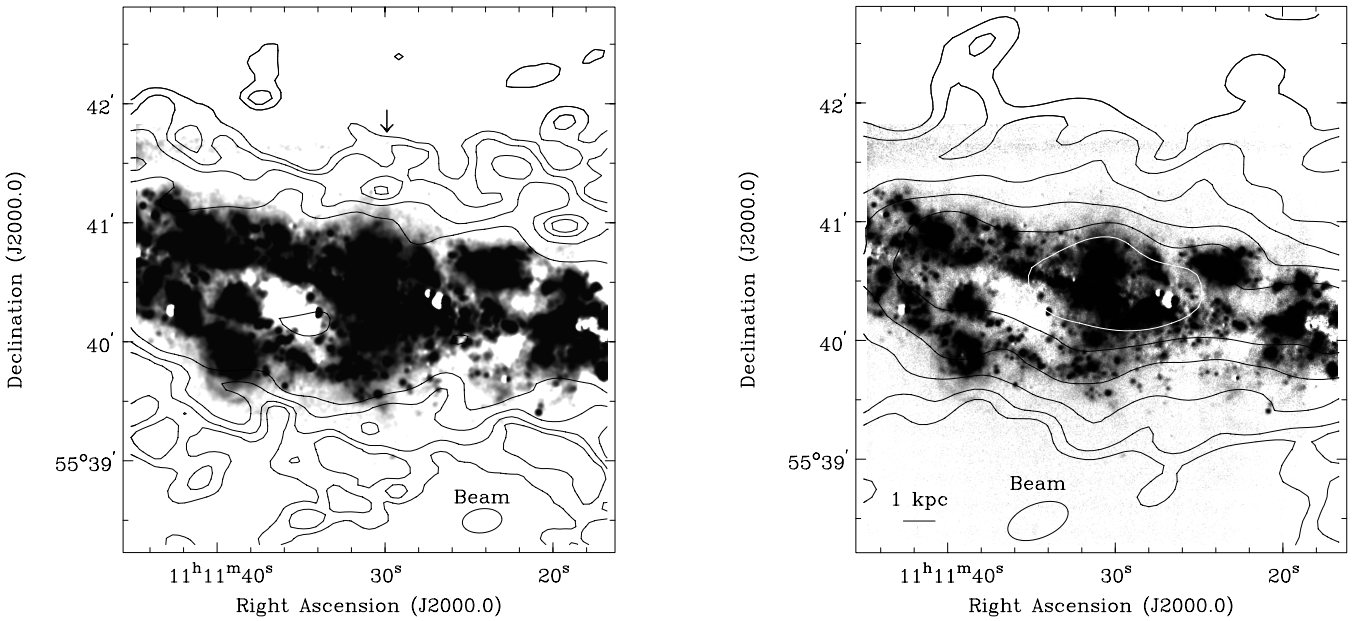

FIG. 11*a* FIG. 11*b*

FIG. 11.—Hα image of NGC 3556 (*a*) smoothed to 1.″5 resolution and (*b*) unsmoothed, with contour overlays of (*a*) H I emission and (*b*) 6 cm radio continuum emission. Closed contours within the feature indicated with an arrow in the H I overlay represent a decrease in column density. Contours for the H I map are 1, 2, 4, and 8 times 324 Jy Hz beam^{-1}. Contours for the radio continuum map are 1.1, 2.2, 4.4, 8.9, 17.8, and 35.6 times 100 μJy beam^{-1}.

TABLE 3

PROFILE SCALE HEIGHTS

Galaxy	Profile Description	DIG Scale Height (kpc)	20 cm Scale Height (kpc)	H I Scale Height (kpc)
NGC 5775.....	NE Hα filament	3.0	2.0	...
NGC 5775.....	0–2 kpc (N)	0.8	1.3	...
NGC 5775.....	8–10 kpc (S), west side	0.9	1.3	...
NGC 5775.....	8–10 kpc (S), east side	0.9	1.2	...
NGC 5775.....	SW Hα filament	2.5	1.4	...
NGC 5775.....	NW 20 cm filament	1.7	2.5	...
NGC 5775.....	SE Hα filament	2.5	1.6	...
NGC 3044.....	W Hα filament	2.0	...	1.8
NGC 3044.....	0–2 kpc (E), north side	1.4	...	1.5
NGC 3044.....	0–2 kpc (E), south side	1.1	...	1.6
NGC 3044.....	0–1.5 kpc (W)	1.1	...	1.4

However, the prominent southern Hα loop at $R = 3$ kpc east of center is spatially correlated with an H I spur. It is difficult to tell whether either of these features are extraplanar or whether they lie in the disk. Though the radio continuum halo is prominent in this region, the loops do not appear to be associated with a radio spur. The DIG filaments extending above the central region of the disk appear to be correlated with a large H I shell, indicated with an arrow in Figure 11, though the shell is not identified as expanding by King & Irwin (1997). A spur of radio continuum emission also appears to be associated with the filaments. However, there are many H I features and radio continuum spurs that do not have a DIG counterpart. In addition, the small field of view of our image does not include the edges of the disk. Thus, we are unable to find DIG counterparts to the highly energetic features identified by King & Irwin as the "eastern" and "western" H I supershells.

5.2. *Scale Heights of Extraplanar Features*

In this section, we compare the vertical extent of Hα, H I, and 20 cm radio continuum emission perpendicular to the major axes of NGC 5775 and NGC 3044. Again, the low inclination of NGC 3556 prevents a detailed analysis of emission scale height. For regions of interest, vertical profiles covering the radial extent of the region are extracted and averaged over that range. We concentrate on modeling areas where a prominent extraplanar feature is apparent in all three tracers, though we do model other regions as well. In comparing scale heights of a certain feature, we attempt to obtain vertical profiles covering the same radial range in all three tracers. In some cases, however, DIG and radio continuum filaments are not perfectly aligned, resulting in vertical profiles extracted from slightly different regions.

Our approach is similar to that used in the modeling of § 4. The method considers a model with a single exponential in the z-direction, of which the peak and scale height, H, can be varied. The model is placed at the inclination quoted in Table 2, and a model profile is generated, which we attempt to fit by eye to the data. For the Hα profiles, we attempt, as before, to fit the model to the data above the H II region layer. DIB98 found that radio continuum emission profiles of NGC 5775 can be fitted only by a superposition of a disk component of small scale height and a halo component of greater extent. Thus, we attempt to fit the 20 cm radio continuum emission profiles in regions above where the disk component may contribute to the total emission.

Results of the modeling are listed in Table 3. Three of the profiles taken from NGC 5775 are of features we have identified as possible chimneys: the northeast filament, the southwest filament, and the southeast filament. Hα, 20 cm, and H I profiles of the northeast filament are shown in Figure 12. The profiles taken from the regions $R = 0$–2 (north) and $R = 8$–10 kpc (south), modeled previously in § 4, are areas where the DIG layer is relatively smooth in appearance. We also model a region with a very prominent radio continuum filament, extending to the west at $R = 6$ kpc north of center, where only low-level extraplanar Hα emission is detectable. Profiles of this region are shown in Figure 13. Our models show that the DIG emission generally has a greater scale height than radio continuum emission for the prominent DIG filaments in NGC 5775. It is clear, however, that the scale height of the radio continuum halo is greater in regions without prominent DIG filaments. H I profiles taken from this galaxy seem to be poorly fit by an exponential distribution. However, the rapid fall-off of H I column density at high z does suggest that neutral hydrogen does not extend as high as DIG filaments or radio continuum emission.

For NGC 3044, we model the west filament, as well as the widespread, smooth layer of DIG above the central region of the galaxy. Profiles of the west filament are shown in Figure 14. Our modeling shows DIG and H I emission are of comparable scale height in NGC 3044 where extraplanar DIG is present. Twenty cm scale heights could not be reliably determined because of significant negative data values in that image, such as in Figure 14*b*.

6. DISCUSSION

6.1. *Diffuse Ionized Gas*

We have found that both NGC 5775 and NGC 3044 have significant extraplanar layers of DIG. The NGC 5775 layer is concentrated in bright, extended filaments, while the DIG in NGC 3044 is confined mainly above the central region of the disk. The smooth appearance of the DIG in NGC 3044 compared with that of NGC 5775 is not a resolution problem, as the galaxy is in fact closer than NGC 5775. We have found that the smooth component of NGC 3044's DIG layer has a larger scale height than that of NGC 5775. NGC 3044 does presumably have a lower mass, however, as its rotational velocity, $V_{\rm rot} = 150$ km s^{-1} (Lee & Irwin 1997), is less than that of NGC 5775, where $V_{\rm rot} = 198$ km s^{-1} (Irwin 1994). Its lower mass should allow material to be lifted higher into its halo. In each of these two galaxies, the

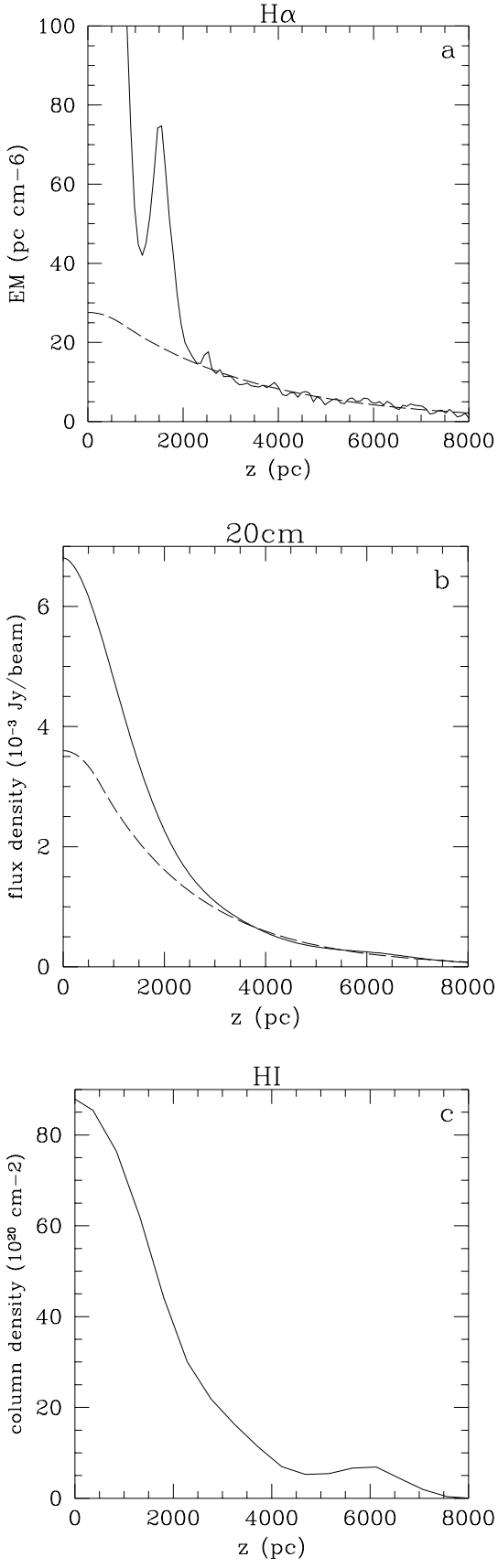

FIG. 12.—Vertical profiles of the northeast Hα filament of NGC 5775. (*a*) Hα profile of the northeast Hα filament (*solid line*) and a model with $H = 3$ kpc (*dashed line*). (*b*) 20 cm profile of the northeast Hα filament (*solid line*) and a model with $H = 2$ kpc (*dashed line*). (*c*) H I profile of the northeast Hα filament (*solid line*). The profile could not be fitted by an exponential distribution.

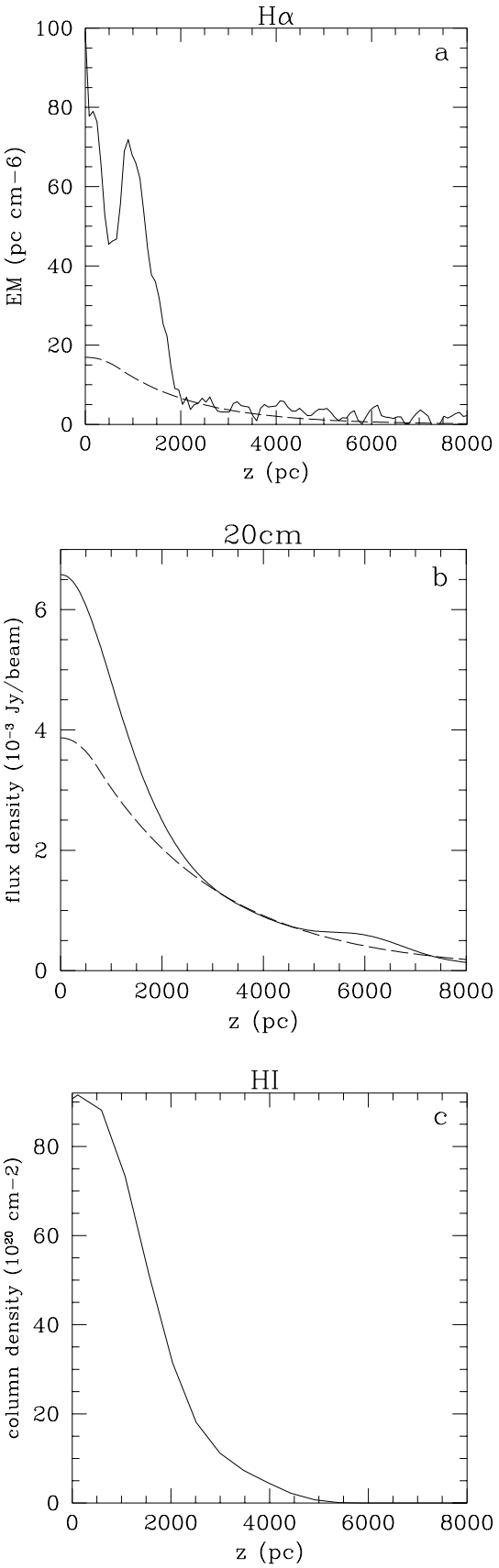

FIG. 13.—Vertical profiles of the northwest 20 cm filament of NGC 5775. (*a*) Hα profile of the northwest 20 cm filament (*solid line*) and a model with $H = 1.7$ kpc (*dashed line*). (*b*) 20 cm profile of the northwest 20 cm filament (*solid line*) and a model with $H = 2.5$ kpc (*dashed line*). (*c*) H I profile of the northwest 20 cm filament (*solid line*). The profile could not be fitted by an exponential distribution.

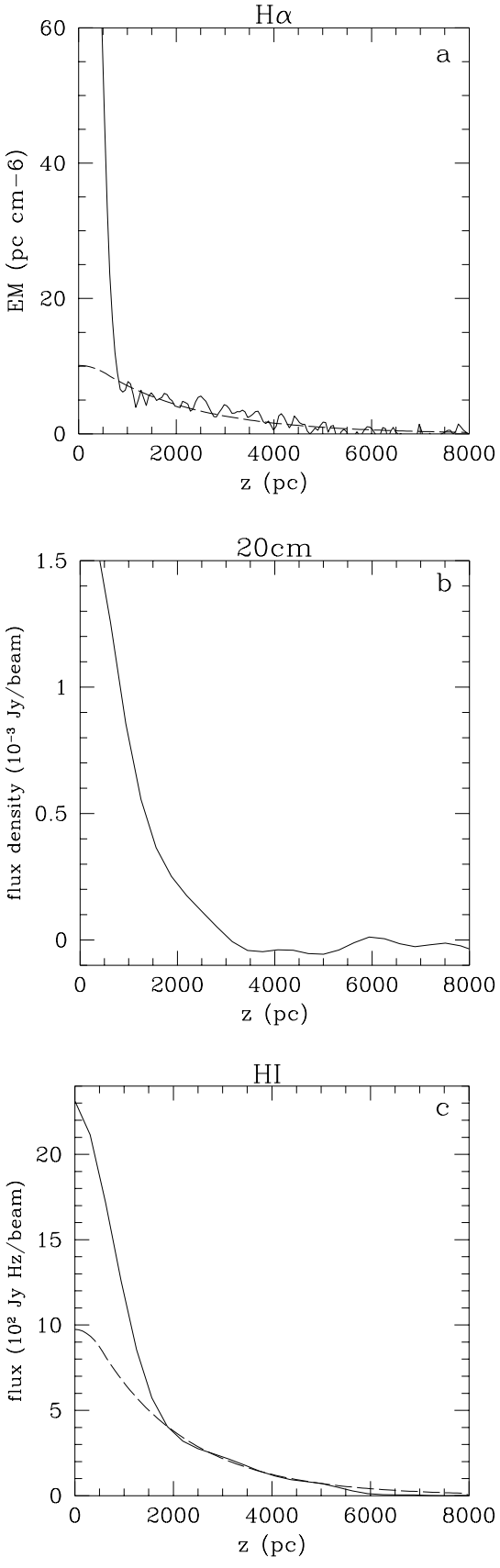

FIG. 14.—Vertical profiles of the west Hα filament of NGC 3044. (*a*) Hα profile of the west Hα filament (*solid line*) and a model with $H = 2$ kpc (*dashed line*). (*b*) 20 cm profile of the west Hα filament (*solid line*). The profile could not be reliably modeled because of significant negative values in the data. (*c*) H I profile of the west Hα filament (*solid line*) and a model with $H = 1.8$ kpc (*dashed line*).

scale height of the DIG layer is greater than that of the Reynolds layer. In contrast, NGC 4183 does not show an extended layer of DIG with parameters comparable to the Reynolds layer, though one plume of DIG is visible. The low inclination of NGC 3556 prevents a detailed study of a possible DIG layer, though a few features are visible.

In Table 2 we have included the far-infrared luminosity ($L_{\rm FIR}$) from the *IRAS* satellite as a tracer of the galaxies' star formation rate (SFR). As an SFR tracer, $L_{\rm FIR}$ has the disadvantage that a portion of the emission seems to be due to a "cirrus" component, heated by an interstellar radiation field arising from stars of a variety of ages (Sauvage & Thuan 1992). $L_{\rm FIR}$ is still the best tracer in edge-ons, however, as Hα luminosity suffers from the very uncertain correction necessary for extinction. Following Rand (1996), we also include the "far-infrared surface brightness," $L_{\rm FIR}/D_{25}^2$, where D_{25} is the optical isophotal diameter at 25th magnitude, as an indicator of the SFR per unit area.

It is clear, then, that the galaxies with the highest SFR per unit area, NGC 5775 and NGC 3044 (ignoring NGC 3556), exhibit prominent extraplanar DIG features. NGC 4183, which shows little extraplanar emission, cannot be included in this comparison, as it was not included in the *IRAS* survey. This result adds further evidence to the correlation between SFR per unit area and extraplanar DIG occurrence, first noted by Walterbos (1991), RKH92, and Dettmar (1992), then expanded on by Rand (1996). This correlation is expected if stellar winds and supernovae are responsible for raising large amounts of gas off the midplane and if OB stars in the disk are then able to ionize this gas, although other star formation–related sources of ionization such as shocks may contribute. It then follows that the level of star formation at a particular part of the disk has a direct influence on the appearance of DIG above. We see such a connection in our data where prominent DIG filaments often connect to locally bright regions of radio continuum emission in the disk. In addition, such a relation is observed NGC 891 where most DIG filaments join onto bright H II regions in the disk (Rand 1997a). However, such connections may not always be observable because of extinction in the disk, confusion from unrelated star-forming regions along a given line of sight, and the possibility that star formation ceased during production of the chimney. Galaxies such as NGC 4183 do not have sufficient star formation activity to power a detectable halo. The one extraplanar Hα feature may mark a local region of relatively intense star formation activity.

6.2. *Correlations with Radio Features*

Comparisons between our Hα images and available radio maps have revealed some interesting results. A "chimney" model of the ISM suggests Hα emission should have associated emission in other tracers. However, outside of galactic nuclei, only in the case of NGC 5775 have such small-scale correlations been found previously, where Hα and radio continuum filaments were found to coincide (Dettmar 1992). Our results have, for the first time, found correlations on the scale of individual filaments between Hα, H I, and radio continuum emission in a galactic disk. The prominent DIG shell on the northeast side of NGC 5775 in particular, which is well correlated with an H I feature and a radio continuum spur, is the most likely candidate for a chimney. NGC 3044 shows similar correlations between the various phases of the ISM, though its extraplanar DIG is fairly

smooth in appearance. NGC 3556, though showing many H I and radio continuum features, shows little extraplanar DIG. A definitive comparison of the galaxy's ISM phases is very difficult because of its low inclination, though in one case we did find correlations between all three tracers. The far-infrared surface brightness of NGC 3556, however, is comparable to that of NGC 3044. Thus, one should expect a significant layer of extraplanar DIG, most of which would not be visible beyond the H II region layer at such a low inclination.

It should be noted that the features we have identified as chimneys are of significantly larger diameter than those predicted by Norman & Ikeuchi (1989). The large size of these structures may simply reflect the most energetic examples of chimney phenomena. The Hα image of NGC 5775 does in fact show many smaller diameter DIG features, lacking H I and radio continuum counterparts, that more closely resemble the structures predicted by the model. The absence of multiwavelength correlations for the smaller features is mainly a selection effect due to poor resolution and sensitivity of the radio maps compared to the Hα image.

The correlation between the prominence of the DIG layer and star formation activity in the disk is strengthened by our multiwavelength comparison as well. The attempt to correlate extraplanar Hα emission with activity in the disk is hampered by extinction. Radio continuum emission, unattenuated by dust in the disk, could then be an excellent indicator of star-forming regions. In both NGC 5775 and NGC 3044, bright regions of radio continuum emission in the disk, outside of the nuclear region, occur directly below a number of prominent DIG filaments. It is possible, however, that these hot spots could be marking areas where the line of sight runs tangent to a spiral arm. In this case one would be making the more general correlation between extraplanar DIG and spiral arms, instead of actual star-forming regions within them. Either way, these hot spots still mark enhancements in the SFR.

In some cases, features of one ISM phase do not have counterparts in other ISM phases. This occurs mainly in NGC 3044, where features identified as H I supershells sometimes lack a DIG counterpart. One would expect such a supershell to be associated with a bright Hα filament or shell if the H I shell has achieved blowout and formed a chimney. An oversubtracted continuum is a possible culprit, though filamentary structure is relatively easy to identify in the presence of small continuum subtraction errors. A lack of ionizing stars in the disk below could also be responsible, as the timescale associated with the lifetime of a chimney could be greater than that of an OB association. Perhaps the gas in the chimney is simply too hot. Also, a pure "chimney" model is perhaps an oversimplification of the complex processes that occur in the ISM and may not explain all occurrences of extraplanar gas.

6.2.1. *Diffusion of CR Electrons into Halo*

For NGC 5775, we have found that extended DIG filaments are correlated with steep spectral index radio continuum emission. Steep spectral indices are expected when the CR transport is dominated by diffusion. In this section we explore the possibility of cosmic rays diffusing into the halo through these chimneys.

According to CR transport theory, relativistic electrons propagate at or near the Alfvén velocity in any frame in which they are fully scattered and in which they establish an isotropic distribution (e.g., Wentzel 1974). The Alfvén velocity is given by

$$V_{\rm A} = \frac{B}{\sqrt{4\pi\rho_i}}\,, \tag{1}$$

where ρ_i is the mass density of the ionized medium through which the electrons are propagating and B is the strength of the ambient magnetic field.

As the electrons propagate, they lose energy through synchrotron radiation and through interactions with ambient photons, through the inverse Compton process. Taking the total energy density of the magnetic field and ambient photons,

$$U_T = \frac{B^2}{8\pi} + U_*\,,$$

the energy loss timescale for an electron is then

$$\tau_e = 3 \times 10^8 \left(\frac{U_T}{\rm eV\,cm^{-3}}\,\frac{E}{\rm GeV}\right)^{-1} {\rm yr}\,, \tag{2}$$

where E is the kinetic energy of the electron (e.g., DIB98).

By combining equations (1) and (2) it is possible to define the propagation scale length. The photon energy densities are difficult to estimate in NGC 5775. However, as we will see, including the photon field only strengthens our conclusions, and we therefore proceed by ignoring the photon contribution to the losses. Combining equations (1) and (2),

$$d \approx V_{\rm A}\,\tau_e = 23\left(\sqrt{\frac{n_i}{\rm cm^{-3}}}\,\frac{B}{\mu\rm G}\,\frac{E}{\rm GeV}\right)^{-1} {\rm kpc}\,. \tag{3}$$

To determine densities within the chimneys we consider the fit to the northeast DIG filament from § 5.2. The fit to the profiled region was characterized by an average squared midplane number density of $\langle n_e^2\rangle_0 = 0.0015$ cm^{-6}. If we assume the filling factor is unity along the line of sight, the average density, above the disk, of the profiled region is ≈ 0.04 cm^{-3}. We take this as the ambient density above the disk for regions outside DIG filaments. To determine the density within the filament we scale the profile density by the ratio of the filament's radial extent to the length of the profile along the disk. We take the filling factor within the filament to be unity. We estimate the gas densities in the filaments to be ≈ 0.3 cm^{-3}. Typical magnetic field strengths were estimated using equiparition calculations (see DIB98). Typically, $B \approx 3$ μG, assuming a cosmic-ray proton to electron ratio of 40. The characteristic energy of an electron radiating in such a field at 1.4 GHz is 13 GeV.

If one assumes that the peak in the electron emission spectrum corresponds to the observing frequency, then the critical frequency is higher than the observing frequency by roughly a factor of 3. This assumption should be correct on average. The number 13 GeV was determined by setting $0.29 \times \nu_c$ (where ν_c is the critical frequency) equal to the observing frequency. Furthermore, the formula for the critical frequency also includes a pitch-angle term. We have assumed a random distribution of electron trajectories in determining the electron energy.

Substituting the above parameters into equation (3) yields characteristic propagation distances of 3.0 kpc for $n_e \approx 0.04$ cm^{-3} and 1.0 kpc for $n_e \approx 0.3$ cm^{-3}. It would seem that, on average, CR electrons can diffuse through the halo to a distance of 3 kpc or so before losing most of their

energy. Such propagation distances are consistent with the measured synchrotron scale heights of the halo (DIB98). Within a filament, where the ionized gas densities are greater, the CR electrons can propagate only about 1 kpc or so. The observed association of the steepest spectral indices with the Hα filaments suggests that the CR electrons have undergone significant energy losses in these regions. Such energy losses are consistent with the estimated value of the propagation distance of 1 kpc.

In the context of diffusion/convection models, a flatter spectral index is often taken to be indicative of winds (e.g., Lerche & Schlickeiser 1982a, 1982b) or a dynamical halo such as the one described by Pohl & Schlickeiser (1990a, 1990b). The observations presented in this paper are not consistent with convective propagation because of the association of steep-spectrum emission with the Hα filaments. However, the flat-spectrum "tentacles" previously reported by DIB98 may still represent convective channels. As noted earlier, they do not have prominent Hα counterparts.

It is therefore concluded that, while convective chimneys of CR electrons may exist, the primary transport mechanism associated with the Hα filaments is diffusive.

This work would not have been possible without support from the staffs at Kitt Peak National Observatory and Apache Point Observatory. Thanks go to Charles Hoopes for calibrating the NGC 3556 data. We would also like to thank Siow-Wang Lee and Judith Irwin for providing the radio data for NGC 3044. This research has made use of the NASA/IPAC Extragalactic Database (NED). This work was partially supported by NSF grant AST96-17014.

REFERENCES

Bloemen, H., Duric, N., & Irwin, J. A. 1993, Proc. 23d Int. Cosmic-Ray Conf., Vol. 2 (Calgary), 279 (BDI93)
Bregman, J. N., & Houck, J. C. 1997, ApJ, 485, 159
Bregman, J. N., & Pildis, R. A. 1994, ApJ, 420, 570
Brinks, E., & Bajaja, E. 1986, A&A, 169, 14
Byun, Y. I., Freeman, K. C., & Kylafis, N. D. 1994, ApJ, 432, 114
Dahlem, M., Dettmar, R.-J., & Hummel, E. 1994, A&A, 290, 384
Dettmar, R.-J. 1992, Fundam. Cosmic Phys., 15, 143
Deul, E. R., & den Hartog, R. H. 1990, A&A, 229, 362
de Vaucouleurs, G., de Vaucouleurs, A., Corwin, H. G., Buta, R. J., Paturel, G., & Fouqué, P. 1991, Third Reference Catalog of Bright Galaxies (New York: Springer)
Duric, N., Irwin, J., & Bloemen, H. 1998, A&A, 331, 428 (DIB98)
Ferguson, A. M. N., Wyse, R. F., & Gallagher, J. S. 1996, AJ, 112, 2567 (FWG96)
Heiles, C. 1979, ApJ, 229, 533
———. 1984, ApJS, 55, 585
Hoopes, C. G., Walterbos, R. A. M., & Greenwalt, B. E. 1996, AJ, 112, 1429
Hoopes, C. G., Walterbos, R. A. M., & Rand, R. J. 1999, ApJ, 522, 669
Irwin, J. A. 1994, ApJ, 429, 618
King, D., & Irwin, J. A. 1997, NewA, 2, 251
Lee, S.-W., & Irwin, J. A. 1997, ApJ, 490, 247
Lerche, I., & Schlickeiser, R. 1982a, MNRAS, 201, 1041
———. 1982b, A&A, 107, 148
Norman, C. A., & Ikeuchi, S. 1989, ApJ, 345, 372
Pohl, M., & Schlickeiser, R. 1990a, A&A, 234, 147
Pohl, M., & Schlickeiser, R. 1990b, A&A, 239, 424
Rand, R. J. 1996, ApJ, 462, 712
———. 1997a, ApJ, 474, 129
———. 1997b, in Gas Disks in Galaxies, ed. J. M. van der Hulst (Dordrecht: Kluwer), 105
———. 1998, ApJ, 501, 137
Rand, R. J., Kulkarni, S. R., & Hester, J. J. 1990, ApJ, 352, L1
———. 1992, ApJ, 396, 97 (RKH92)
Rand, R. J., & van der Hulst, J. M. 1993, AJ, 105, 2098
Reynolds, R. J. 1993, in AIP Conf. Proc. 278, Back to the Galaxy, ed. S. S. Holt & F. Verter (New York: AIP), 156
Reynolds, R. J., & Tufte, S. L. 1995, ApJ, 439, L17
Sauvage, M., & Thuan, T. X. 1992, ApJ, 396, L69
Slavin, J. D., Shull, J. M., & Begelman, M. C. 1993, ApJ, 407, 83
Sorathia, B. 1994, M.S. thesis, Queen's Univ.
Swaters, R. A., Sancisi, R., & van der Hulst, J. M. 1997, ApJ, 491, 140
Tully, R. B. 1988, Nearby Galaxies Catalog (Cambridge: Cambridge Univ. Press)
Walterbos, R. A. M. 1991, in IAU Symp. 144, The Interstellar Disk-Halo Connection in Galaxies, ed. J. B. G. M. Bloemen (Dordrecht: Kluwer), 223
Walterbos, R. A. M., & Braun, R. 1994, ApJ, 431, 156
Wang, Q. D., Walterbos, R. A. M., Steakley, M. F., Norman, C. A., & Braun, R. 1995, ApJ, 439, 176
Wentzel, D. G. 1974, ARA&A, 12, 71